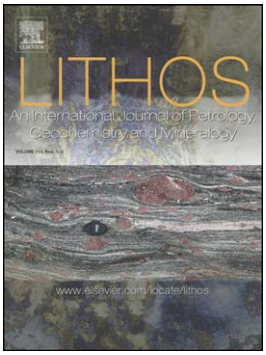

$^{40}Ar/^{39}Ar$ ages and petrogenesis of the West Iberian Margin onshore magmatism at the Jurassic-Cretaceous transition: Geodynamic implications and assessment of open-system processes involving saline materials

J. Mata, C.F. Alves, L. Martins, R. Miranda, J. Madeira, N. Pimentel, S. Martins, M.R. Azevedo, N. Youbi, A. De Min, I.M. Almeida, M.K. Bensalah, P. Terrinha

PII: S0024-4937(15)00308-4
DOI: doi: 10.1016/j.lithos.2015.09.001
Reference: LITHOS 3678

To appear in: *LITHOS*

Received date: 11 September 2014
Accepted date: 2 September 2015

$^{40}Ar/^{39}Ar$ ages and petrogenesis of the West Iberian Margin onshore magmatism at the Jurassic-Cretaceous transition: geodynamic implications and assessment of open-system processes involving saline materials

J. Mata[1*]; C.F.Alves[1]; L. Martins[1]; R. Miranda[1]; J. Madeira[1]; N. Pimentel[1]; S. Martins[1]; M.R. Azevedo[2]; N. Youbi[3,1]; A. De Min[4]; I. M. Almeida[1]; M.K. Bensalah[3,1]; P. Terrinha[5]

[1] Instituto Dom Luiz, Faculdade de Ciências, Universidade de Lisboa, 1749-016 Lisboa, Portugal

[2] Universidade de Aveiro, Departamento de Geociências, and GEOBIOTEC, Campus Santiago, 3810-193 Aveiro, Portugal

[3] Geology Dept., Fac. of Sciences-Semlalia, Cadi Ayyad University, Prince Moulay Abdellah Boulevard, P.O. Box 2390, Marrakech, Morocco.

[4] Università degli Studi di Trieste, Dipartimento di Scienze Geologiche, via E.Weiss 8, 34127 Trieste, Italy.

[5] IPMA – Instituto Português do Mar e da Atmosfera, Lisboa, Portugal

*__Corresponding author:__ Departamento de Geologia da Faculdade de Ciências da Universidade de Lisboa. Campo Grande C6. 149-016 Lisboa, Portugal.

jmata@fc.ul.pt

Phone: +351 938515021

Abstract

The West Iberian Margin (WIM) preserves onshore testimonies of three Mesozoic magmatic cycles. In this paper, we present and discuss $^{40}Ar/^{39}Ar$ ages and geochemical data for the second cycle, which occurred at least from 148 Ma to 140 Ma, at the Jurassic-Cretaceous transition, during the late stages of an important extensional event associated with the Iberia-Newfoundland rifting. The related lithospheric stretching induced magma genesis by adiabatic decompression. Primitive rocks are fairly alkaline but evolved to SiO_2-saturated and oversaturated rocks at "high" pressure. Magmas sampled a source of fairly homogenous composition characterized by Sr and Nd isotopic compositions (εNd_i from +1.6 to +4.2), more enriched than the typical N-MORB source. Magmas were generated at the top of the garnet zone. Considering the thickness of the lithosphere and the geochemical constraints, an origin by melting of a metasomatized domain of the lithosphere is favoured. The composition of these onshore magmas is somewhat distinct from the quasi coeval magmas emplaced offshore, which is interpreted as a result of the less important onshore lithospheric stretching, leading to lower degrees of partial melting. This favoured the contribution of lithospheric metasomatized domains to onshore magmas. Rocks intruded two sectors of the Lusitanian Basin separated by the Nazaré Fault and characterized by distinct subsidence rates during the Jurassic. The fact that the rocks to the north of the Nazaré Fault are significantly more evolved indicates the more important development of magma chambers in the north, suggesting distinct thermal profiles for those two sectors. Such magma chambers enabled the "high-pressure" fractionation necessary to drive magma compositions from Ne-normative to SiO_2- saturated and -over-saturated. The rocks cropping out south of the Nazaré fault are clearly less evolved, and its variability is mostly due to different partial melting events. Some rocks present evidence of post-

magmatic processes involving neighbouring Jurassic evaporite materials, leading to an increase in the Na_2O content and $^{87}Sr/^{86}Sr$ ratio.

1. Introduction

It has long been recognized that a correlation exists between tectonic setting and the geochemistry of the associated magmas. This confers an important role to the study of magmatic rocks when assessing heat and mass transfer processes between the Earth mantle and crust, as well as in deciphering the geodynamic evolution of the lithospheric sector where they occur. Particularly interesting is the intraplate magmatism due to the variety of processes involved in its genesis and the possibility of having lithospheric or sub-lithospheric (asthenospheric and/or plume) sources.

The last major reorganization of the Earth's lithospheric plates started in the Triassic, with the fragmentation of Pangea, which led to the birth of the Atlantic Ocean. With the progressive opening of the Atlantic, Mesozoic sedimentary basins developed adjacent to the Palaeozoic Iberian Massif, later evolving into passive continental margins (e.g., Sibuet et al., 2007; Tucholke et al., 2007; Bronner et al., 2011). At the West Iberian Margin (WIM), the extension associated with the oceanization propagated northward, a process that occurred in a step-wise manner (e.g., Tucholke and Whitmarsh, 2012; Afilhado et al., 2008) at a mean rate of approximately 4.4 $cm.a^{-1}$ between the Gorringe and Galicia banks (Scharer et al., 2000).

Although the WIM is usually described as a non-volcanic or magma-poor margin, characterized by the absence of typical seaward-dipping reflectors and significant magnetic anomalies and by the occurrence of exhumed mantle portions (e.g., Pinheiro et al., 1996; Whitmarsh et al., 2001; Jagoutz et al., 2007; Reston et al., 2009; Bronner et al., 2011; Minshull et al., 2014), magmatic occurrences are known both offshore and onshore (e.g., Rock, 1982; Scharer et al., 2000; Merle et al., 2006). On the onshore portions of the Mesozoic basins (Algarve, Alentejo and Lusitanian) of the West Iberian Margin, three magmatic cycles were identified, separated by intervals of ≈50 Ma of

quiescence and characterized by different geochemical signatures (e.g., Ribeiro et al., 1979; Ferreira and Macedo, 1983; Martins, 1991; Pinheiro et al., 1996; Martins et al. 2010). The existence of these three cycles, spanning from ≈ 200 Ma to ≈70 Ma, offers an opportunity to use magmatic signatures to constrain the ≈ 130 Ma evolution of a continental margin, from the initial stages of rifting to the passive margin stage.

The ages of the first (202-198 Ma; Rapaille et al., 2003; Verati et al., 2007) and third (94 to 69 Ma; Miranda et al., 2009; Grange et al., 2010) cycles recognized at the WIM onshore are reasonably well known, as are their petro-chemical characteristics (see Cebriá et al., 2003; Martins et al., 2008; Miranda et al., 2009; Grange et al., 2010; Callegaro et al., 2014 and references therein). These authors demonstrated the tholeiitic signatures of the first cycle, which is considered coeval with the beginning of the Central Atlantic opening and a part of the Central Atlantic Magmatic Province (CAMP; Marzoli et al., 1999). For the third cycle, an alkaline character was assigned (see also Alves et al., 1980; Rock, 1982). This cycle was partially contemporaneous with the Bay of Biscay break-up and the associated counter-clockwise rotation of Iberia, as well as of the occurrence of significant magmatism offshore (Merle et al., 2006; Merle et al., 2009) and at Northeast Iberia (e.g., Ubide et al., 2014).

Less well known is the second magmatic cycle, whose testimonies are only preserved in the Lusitanian Basin (LB) in two sub-meridional alignments occurring between the latitudes of Rio Maior and Soure (Fig. 1). In the last four decades, the magmatic rocks generated during this cycle were the main subject of one single publication (Grange et al., 2008). The present paper aims to contribute to filling this gap by presenting and discussing three new $^{39}Ar/^{40}Ar$ ages and major and trace element analyses of 17 selected samples, 10 of which were also analysed for Sr and Nd isotopes. Our main objectives are (1) to clarify the duration of this cycle, (2) to better constrain the geochemical

affinities of the magmatic rocks, (3) to determine the causes of the observed geochemical variability, (4) to discuss the geodynamic significance of magmatism and (5) to compare the obtained results for the second magmatic cycle with those from the other onshore Mesozoic cycles, discussing the temporal evolution of the Western Iberian magmatic sources/processes throughout ≈130 Ma. We will also demonstrate the occurrence of post-magmatic processes involving the participation of Early Jurassic evaporites occurring in close spatial relation with the magmatic rocks.

2. Geological setting

When the Pangea breakup started, the Iberian microplate was located near the Western Tethys. Subsequently, it was subjected to a complex evolution constrained by the relative motion of the surrounding Eurasian, African and North American lithospheric plates (e.g., Pinheiro et al., 1996).

During the Mesozoic, a series of peripheral rift basins with somewhat distinct tectonostratigraphic histories formed around Iberia (e.g., Terrinha et al., 2002; Carvalho et al., 2005; Alves et al., 2009; Pereira and Alves, 2011), associated with i) the intra-continental rifting between Newfoundland and Eurasia and ii) the southeastward-directed drifting of Africa with respect to Eurasia, at the western end of the Tethys Ocean.

The Lusitanian Basin (LB), in the West Iberia, Margin (WIM), from where the studied rocks were sampled, is one such peri-Atlantic basin and is presently one of the few exposed onshore, allowing the direct observation of the sedimentary sequences on outcrops (e.g., Pena dos Reis et al., 2011). This, associated with the potential occurrence of hydrocarbons (e.g., Uphoff, 2005; Duarte et al., 2012), resulted in many studies of its origin and evolution (Ribeiro et al., 1979; Wilson et al., 1989; Pinheiro et al., 1996;

Rosenbaum et al., 2002; Azerêdo et al., 2002; Alves et al., 2009; Pena dos Reis et al., 2011; Pereira and Alves, 2012; Kullberg et al., 2013; Pena dos Reis and Pimentel, 2014).

The Mesozoic extensional regime linked to the opening of the North Atlantic Ocean was the main constraint in the generation and evolution of the LB, which evolved from a rift-related Triassic intracontinental basin, with alluvial redbeds (Silves Formation) and marginal sabkha environments (evaporites and clays of the Dagorda Formation), to a Jurassic open marine carbonate platform (e.g., Azerêdo et al., 2002). During Aptian-Albian times, the breakup unconformity formed after the complete separation of the lithosphere and the emplacement of the true oceanic crust (e.g., Soares et al., 2012 and references therein).

Sub-division into sub-basins, i.e., the location of sedimentary depocentres, was controlled by the main basement faults, which also served as localization for the main salt walls and magma conduit ascent channels (Fig. 1). The Nazaré Fault and Tagus valley faults sub-divided the LB into three sectors, whilst the Porto-Tomar, Arrife and Arrabida valley faults bounded the LB. It is of general agreement that the two main periods of accelerated extension (i.e., rifting events; altogether between two and four, according to different authors) occurred in Triassic-Hettangian and Late Jurassic times (e.g., Rasmussen et al., 1998; Kullberg et al., 2013). The latter predated and was partially coeval of the second magmatic cycle. Afterwards, a phase of the general uplifting of the WIM occurred, with siliciclastic fluvial progradation (e.g., Dinis et al., 2008). See Fig. 2 for a stratigraphy synthesis.

The testimonies of the second Mesozoic magmatic cycle in the LB are preserved both in the North and Central sectors (Fig. 1). In fact, their main occurrences (mostly sills and dikes) are concentrated in two sub-meridian alignments, one along the Eastern border of

the basin (Rio Maior-Porto de Mós-Alqueidão da Serra-Vermoil) and the other one to the West (Nazaré-Monte Real-Monte Redondo-Soure), located, respectively, South and North of the Nazaré Fault. There are also a few laccoliths (Northern sector) and dykes sub-perpendicular to the basin axis (central sector). Extrusive rocks have not been reported so far. Magmatic bodies are spatially associated with Hettangian saline-rich deposits exhumed by diapirism, suggesting a common tectonic control of both magmatic and saline ascension by the same pre-existing fault systems (Ribeiro et al., 1979; Kullberg et al., 2013; see also section 5.4). The location of the outcrops where the rocks used in the present study were sampled from is shown in Fig. 1, and their geographic coordinates are listed in Supplementary Material - S1. From now on, the studied rocks will be referred to as the Northern rocks or the Southern rocks according to their location relative to the Nazaré Fault.

3. Analytical procedures

$^{40}Ar/^{39}Ar$ age determinations were performed at the Noble Gas Mass Spectrometry Laboratory of the Oregon State University, Corvallis, USA. The material to be analysed was irradiated in the TRIGA reactor for 6 h with 1 MW neutrons, together with the biotite standard FCT-3 (28.03±0.01 Ma age) to monitor the neutron flux and allow the calculation of J parameters. The Ar isotopic ratios were determined with an MAP 215-50 rare gas mass spectrometer. The data obtained were corrected for mass fractionation, interfering Ar isotopes and system blanks. The $^{40}Ar/^{39}Ar$ ages were calculated with ArArCALC software (Koppers, 2002), using a decay constant $\lambda=(5.530\pm0.097)\times10^{-10}$ y^{-1} (Min et al, 2000). As a whole, the methodology is similar to that described by Duncan and Kellers (2004). Further information about the procedure is available on the Oregon

State University website (http://geochronology.coas.oregonstate.edu/), while details on the analysed samples can be found below in section 4.2 (Age determinations).

Mineral chemistry analyses were performed with a JEOL model JXA8200 microprobe housed at Faculdade de Ciências da Universidade de Lisboa. All of the analyses were performed with a 5 μm diameter beam, accelerated by 15 kV tension. Natural and synthetic mineral and purified metal standards were used. The precision, as evaluated from repeated readings on the standards, is better than 2% and approximately 1%.

The samples selected for elemental and isotopic analyses were hammered to small pieces, crushed in a jaw crusher, and finally pulverized using an agate mortar.

Whole-rock major and trace element concentration analyses were performed at ACTLABS, Canada, according to the 4Lithoresearch WRA+Trace package. In fusion processes, the sample is mixed with a flux of lithium metaborate and lithium tetraborate, fused in an induction furnace and then dissolved in a solution of 5% nitric acid. For total digestion, the samples are sequentially treated with acids (first hydrofluoric, then a mixture of nitric and perchloric acids) and then evaporated and dissolved again in hydrochloric acid. Afterwards, the major elements were analysed by inductively coupled plasma-optical emission spectrometry (ICP-OES), while the trace element contents were obtained using inductively coupled plasma-mass spectrometry (ICP-MS) on a Perkin Elmer SCIEX ELAN ICP/MS (with the exception of Sc, V, Ba and Sr, which were obtained by ICP-OES). Blanks are analysed periodically. Reproducibility is verified by analysing duplicates every 15 samples, and the equipment is recalibrated every 40 samples. The obtained reproducibility is better than (i) three relative-% for major elements and (ii) seven relative-% for rare earth elements and elements generally behaving as incompatible. The accuracy, evaluated by analysing international standards, is generally better than 12 relative-%, with the results for many elements within ± 6% of

the recommended values. Additional information on the analytical and control procedures can be found at the ACTLABS website (http://www.actlabs.com).

Sr and Nd isotopic analyses were performed by TIMS at the Laboratório de Geologia Isotópica, Universidade de Aveiro (Portugal). Chemical separation procedures were carried out in a clean room (ISO Class 5). Acids were purified by sub-boiling distillation and diluted to working concentrations with Milli-Q ultra-pure water (18.2 MΩ). Materials and containers were previously decontaminated by immersion in boiling 50% HNO_3 for one day and washed three times in Milli-Q ultra-pure water. Samples showing petrographic evidence of secondary carbonates were leached with 1 N acetic acid. Sample decomposition was achieved by adding a mixture of concentrated HF and HNO_3 acids (2 mL HF + 1 mL HNO_3) to 500 mg of rock powder in pressurized Parr acid digestion vessels, which were then sealed and heated to 180ºC in an oven for three days. The excess HF and volatile SiF_4 were removed by subsequent evaporation of the sample solutions on a hotplate. The residue was taken up in 3 mL 6.2 N HCl, and the vessel was resealed and placed back in the oven for a few hours. Following a subsequent evaporation step, the solid residues were dissolved in 0.4 mL of 2.5 N HCl and loaded into primary chromatographic columns (Bio-Rad AG8 50W resin) for the extraction of Sr and the REEs. The Sr and REE fractions were eluted from the cation exchange columns through the successive addition of predetermined volumes of 2.5 N HCl, 4 N HNO_3 and 6.2 N HCl. Neodymium was separated from the remaining REEs in secondary quartz glass columns filled with LN-resin, supplied by Eichrom Technologies Inc., after elution with 0.2 N HCl and 0.3 N HCl. The collected Sr and Nd solutions were then dried and taken up for TIMS analysis. Sr was loaded on outgassed single Ta filaments with H_3PO_4, and Nd on Ta-Re-Ta triple filaments with diluted HCl. The $^{87}Sr/^{86}Sr$ and $^{143}Nd/^{144}Nd$ isotope ratios were measured on a VG Sector 54 mass

spectrometer operating in dynamic mode, using beam intensities of 1–2 V for ^{88}Sr (50–100 cycles) and 0.5-1 V for ^{144}Nd (50–100 cycles). The Sr and Nd isotopic ratios were corrected for mass fractionation using exponential law corrections ($^{86}Sr/^{88}Sr = 0.1194$; $^{146}Nd/^{144}Nd = 0.7219$). Repeated analysis of international SRM-987 and JNdi-1 standards gave average values of $^{86}Sr/^{88}Sr = 0.710243 \pm 10$ (uncertainty given at 95% confidence level, N=14; literature value = 0.710248 ± 23; Thirlwall, 1991) and $^{146}Nd/^{144}Nd = 0.512105 \pm 4$ (uncertainty given at 95% confidence level; N=18; literature value = 0.512115 ± 8, Tanaka et al, 2000). The external precision (i.e., twice the standard deviation of the mean values for each individual run, 2σ) was estimated from sets of repeated analyses of international standards. Analytical blanks for Sr and Nd are, in both cases, lower than 250 pg.

4. Results

Onshore WIM rocks generated during the second Mesozoic magmatic cycle were previously described/studied from the perspectives of petrography (e.g., Morais and Neiva, 1947; Martins, 1991; see also Grange et al., 2008), geochronology (Ferreira and Macedo, 1983; Grange et al., 2008) and geochemistry (Martins, 1991; Grange et al., 2008). These studies were instrumental in identifying the still unsolved problems so as to encourage research focus on them. Their results will be presented and discussed throughout the text in conjunction with our data.

4.1. Petrography and mineral chemistry

In this chapter, we will emphasize the most relevant petrographic and mineral chemical features of these rocks, which present distinct characteristics as a function of their

geographic location. In fact, as expressed in Fig. 1, the existence of two groups, roughly separated by the ENE-WSW Nazaré Fault, can be considered.

The rocks cropping out south of Nazaré Fault but in close proximity to it (BL19, BL23, BL24; see Fig. 1), correspond to dolerites showing porphyritic textures with aphanitic (BL19) to microphaneritic (BL23, BL24) groundmasses. Their typical primary mineralogy consists of olivine phenocrysts in a cryptocrystalline (BL19) or microcrystalline (BL23, BL24) matrix containing plagioclase, olivine, clinopyroxene and oxides. Some olivine phenocrysts present zoning (e.g., Fo_{core}=84.28 to Fo_{rim}=77.51 in BL19) and/or embayments filled up with groundmass, suggesting boundary corrosion derived from the chemical disequilibrium between crystals and the remnant liquid. Oxides included in olivines are chrome-aluminous spinels (up to 20% Cr_2O_3 and 35% Al_2O_3), clearly distinct from those dispersed in the groundmass (titanomagnetite), as often reported for mafic rocks elsewhere (e.g., Mata and Munhá, 2004 for Madeira Island alkaline basalts). There is no evidence of significant mineral alteration. In the Southern Group, the southernmost cluster of rocks (BL01 to BL08, see Fig. 1) presents intergranular (BL01, BL05) to sub-ophitic (BL03, BL04, BL06, BL07, BL08) textures. Again, the primary minerals are olivine (Fo=86.27 to 59.13), plagioclase (mainly labradorite, An up to 64.89%), clinopyroxene (diopside and magnesium somewhat titaniferous augite, TiO_2 up to 4.72 wt %), with scarce potassium feldspar (Or up to 64%), oxides, biotite and apatite in the interstitial spaces. Olivine and plagioclase sometimes present zoning expressing temperature decreases and the compositional evolution of the magmatic liquid (Fo_{core}=82.71 to Fo_{rim}=59.73; An_{core}=60.31 to An_{rim}=3.49). Secondary minerals are almost restricted to serpentine after olivine (incipient substitution along fractures in BL03, BL04, BL05 and moderate to strong replacement in BL01, BL06, BL07, BL08) and rare chlorite after biotite.

Rocks in the Northern Group are medium to coarse-grained diorites (BL13, BL16) and gabbros (BL14, BL15, BL18, BL21, BL29), with textures ranging from glomeroporphyritic (BL15) and ophitic (BL14) to sub-ophitic for the remaining samples. In this group, the primary minerals are zoned plagioclase, with core to rim compositions ranging from labradorite to andesine (An=57.47 to 44.90%) and oligoclase to albite (An=23.73 to 1.88%); alkaline feldspar, with potassium up to Or_{98} in the most evolved rocks (such as BL13 and BL29); low Ti magnesium augite (TiO_2<1.2%, En=47.20 to 41.79%); oxides (skeletal Fe-Ti oxides, some with exsolution textures where magnetite-rich and ilmenite-rich oxides coexist); scarce amphibole (hornblende), biotite, apatite and significant amounts of titanite (BL18, BL29). Quartz occurs as a primary mineral in the most evolved rocks (BL13, BL16) where it forms, with alkaline feldspars, interstitial graphic intergrowths, which indicates a sub-alkaline magma composition.

An important feature of these Northern samples is the evidence for strong hydrothermal alteration recognized by the presence of zeolites and multiple mineralogical replacements: sericite, in plagioclase rims (BL13, BL14, BL15, BL16, BL21); plagioclases entirely replaced by prehnite (BL18, BL29); actinolite overgrowths in clinopyroxenes (slight in BL21, BL29 and complete pseudomorphoses in BL13, BL14, BL16); replacement of amphibole with biotite and/or chlorite; and hydration of Fe oxides. The observed secondary minerals are consentaneous with the occurrence of hydrothermal alteration under temperature conditions ranging up to those typical of greenschist facies.

The crystallization sequence inferred from the textural analyses is variable. When present, olivine is the first silicate phase to crystallize, while the subsequent order of crystallization depends on the degree of silica saturation, which, as will be shown (e.g.,

Fig. 7a), is highly variable. On silica-undersaturated rocks, clinopyroxene crystallization precedes plagioclase, while in rocks characterized by significant amounts of normative hypersthene, the opposite is observed. Undersaturated rocks are also characterized by the presence of titanomagnetite (s.l.), which, for high-normative hypersthene and oversaturated rocks, is joined by members of the ilmenite-hematite solid solution.

4.2. Age determination

To complement the geochronological data presented by Ferreira and Macedo (1983) and Grange et al. (2008) (see section 5.1), $^{40}Ar/^{39}Ar$ age determinations were performed for three samples, selected according to their geographic location and preservation of magmatic characteristics. The dated samples (BL07, BL19 and BL24) are described in section 4.1 and Table 1. The incremental heating steps were obtained with an electrical oven for sample BL19 (whole-rock) and with a continuous fire CO_2 laser (Merchantec, 10 W) for the plagioclases (samples BL07 and BL24). Thirteen heating steps between 400 and 1400ºC were used for BL19, and eleven heating steps between 500 and 1400ºC were used for BL07 and BL24.

The obtained BL07 and BL24 plateaus contain all or the majority of the total ^{39}Ar released, while for BL19, the obtained plateau (6 out of 13 heating steps) corresponds only to 57.4% of the total ^{39}Ar released, which makes the obtained result somewhat questionable. However, it is generally accepted that in age spectrum diagrams, a plateau is identified when one set of at least three adjacent sections corresponds to more than 50% of the total ^{39}Ar released and when no difference in the apparent age can be detected between any two fractions at the 95% confidence level (e.g., Fleck et al., 1977; Baksi, 2006; Renne et al., 2009). Considering these criteria, the petrographic lack of evidence for significant alteration and their MSDW and p statistical parameters present

values are lower than 2.5 and higher than 0.05, respectively, we consider the result obtained for sample BL19 to be valid.

The obtained results (Table 1) cover a range of 5.22 ± 1.73 Ma, varying between 141.29 ± 0.95 Ma (BL24) and 146.51 ± 0.78 Ma (BL19). For BL07, an age of 144.98 ± 0.73 is assigned (Table 1). These plateau ages are identical, within error, to those that can be deduced from inverse isochrones. The $^{40}Ar/^{36}Ar$ ratios are indistinguishable, within the error range, from the atmospheric value (295.5; e.g., Ozima and Podosek 2002), excluding the possible existence of radiogenic Ar at the system closing temperature. The lower age deduced from the first few heating steps of BL19 and BL24 are considered to reflect the post-crystallization loss of Ar from lattice positions with lower retention energy.

4.3. Major and trace element compositions

Whole-rock sample compositions for major and selected trace elements are reported in Table 1. Mg# was computed as Mg# = 100 Mg / (Mg+Fe^{2+}), with Fe^{2+} calculated from the analysed Fe_2O_3(T), using the Fe_2O_3/FeO ratios recommended by Middlemost (1989) according the positioning of each sample in the TAS diagram (LeBas et al., 1986). In this diagram (Fig. 4), we also plotted the analyses performed by Grange et al. (2008) for three samples, as well as, for comparison purposes, the fields defined by magmatic rocks for the other two Mesozoic cycles identified in the WIM (see 1).

The majority of the samples are basic, except for BL19 (ultrabasic) and BL16, which are slightly more evolved (SiO_2 = 52.10 %). Rocks cropping out north of the Nazaré Fault are clearly more evolved (33.17 < Mg# < 56.13) than the Southern ones (58.81 < Mg# < 67.43). With the exception of the three more evolved Northern rocks, all of the other samples from both groups plot in the basalt field of the TAS diagram (Fig. 4).

Samples range from moderately alkaline to slightly sub-alkaline, plotting close to and on both sides, of the boundary between these fields, as defined by Irvine and Baragar (1971). The total alkali content ($Na_2O + K_2O$) ranges from 3.68 to 4.73 wt. %, with the exceptions of samples BL18 (5.68 wt. %) and BL29 (6.33 wt%), which, as seen at 5.3, are considered to be affected by post-magmatic processes. The most abundant alkali is sodium, which usually translates to $Na_2O/K_2O > 2$. This ratio reaches its maximum values in samples BL18 (6.24) and BL29 (10.48), for which the Na_2O contents (4.68 and 5.66 wt. %, respectively) are also maximal among the studied samples. For one of the samples analysed by Grange et al. (2008), an even higher Na_2O concentration (6.29 wt. %) was determined.

REE patterns (Fig. 5a) show significant fractionation of the LREE compared to the heavy ones. This is noticeable even for the less evolved samples (Ni > 190 ppm) of the Southern rocks, which are characterized by chondrite-normalized La/Yb ratios ranging from 5.91 to 11.32. For the same sub-set of samples, the chondrite-normalized Sm/Yb ranges from 2.54 to 3.82. Taking into account the relatively unevolved characteristics of this set of samples (Ni > 190 ppm), the large ranges of MREE/HREE and LREE/HREE suggest that the analysed rocks are not strictly comagmatic. The elemental compositions normalized to the primitive mantle (Fig. 5b) show stronger enrichment for the most incompatible elements. For example, even for the relatively unevolved (Ni > 190 ppm) Southern rocks, Th is approximately 48 times that of the primordial mantle, while less incompatible elements (e.g., Y) are characterized by enrichment factors of about 5.1 to 5.6. The more evolved Northern rocks are generally more enriched in the most incompatible REE than their Southern counterparts. Some rocks are characterized by small negative Nb anomalies, which are more pronounced on the Northern rocks (Fig. 5).

4.4. Sr and Nd isotopic ratios

A subset of 10 samples was analysed for the Sr and Nd isotopic ratios. The results and the ratios recalculated for 145 Ma, the approximate mean age of the rocks (see sections 4.1 and 5.1), are listed in Table 3 (see also Fig. 6).

The initial $^{87}Sr/^{86}Sr$ ratios range from 0.704034 to 0.704732 in the Southern rocks and from 0.704533 to 0.707034 in the Northern rocks. The $(^{143}Nd/^{144}Nd)_i$ ratios vary between 0.512531 and 0.512664 and from 0.512539 to 0.512592 in the Southern and Northern rocks, respectively. Grange et al. (2008) presented Sr isotopic analyses for three samples, which by their locations can be considered as belonging to the Northern group. Their initial ratios (0.70534 to 0.70646) are within the range of our determinations for the Northern rocks.

The plot of $(^{147}Nd/^{144}Nd)_i$ against $(^{87}Sr/^{86}Sr)_i$ (Fig. 6) shows that the majority of the samples form a cluster with isotopic ratios that do not deviate significantly from the CHUR and UR values, here recalculated for 145 Ma ago. However, three Northern samples (BL18, BL21 and BL29) are exceptions, being clearly more Sr-radiogenic for a given $^{143}Nd/^{144}Nd$, strongly suggesting the incorporation of material with relatively high $^{87}Sr/^{86}Sr$ and/or very rich in ^{87}Rb (see below for a discussion).

Grange et al. (2008) also presented, for the three samples referred to above, lead isotope ratios, which show as the most peculiar characteristic a very high $^{207}Pb/^{204}Pb$ (15.925) for a given $^{206}Pb/^{204}Pb$ (18.978), as determined for one of the samples.

5. Discussion

5.1. Age and duration of the second Mesozoic magmatic cycle in the West Iberian Margin (WIM)

As previously mentioned, the ages of the first (202-198 Ma; Rapaille et al., 2003; Verati et al., 2007) and third (94 to 69 Ma; Miranda et al., 2009; Grange et al., 2010) magmatic cycles at the WIM are considered reasonably well constrained. Less well known are the ages and durations of the second cycle, here under study.

The first isotopic age determinations of rocks belonging to this cycle were published by Ferreira and Macedo (1983), who reported K-Ar ages of 144 to 133 Ma for the Southern rocks and older ages (up to 165 Ma) for the Northern rocks. However, in this case, the authors warned of the altered state of the analysed samples. Subsequently, three Northern rocks were dated by Grange et al. (2008) using U-Pb in titanites, a methodology significantly less prone to alteration processes. They obtained ages (S. Bartolomeu: 146.5±1.6 Ma; Leiria: 142.3±1.0 Ma; Soure: 145.3±1.4 Ma; see Table 4) that are clearly younger than those previously obtained for this group, thus confirming the doubts of Ferreira and Macedo (1983) about the applicability of the K-Ar method to these altered rocks (Table 4). To complement the Grange et al. (2008) data, we performed three new $^{40}Ar/^{39}Ar$ analyses on fresh rocks from outcrops located south of the Nazaré Fault. Our results (Table 1) are similar to those obtained by Grange et al. (2008) for the Northern rocks (Table 4).

Considering the doubts about the validity of the above mentioned K-Ar ages, our $^{40}Ar/^{39}Ar$ data for the Southern rocks and the U-Pb ages presented by Grange et al. (2008) for the Northern ones, we conclude that the magmatic rocks from both groups are coeval. Moreover, the same data set points to an age range from 141.29 ± 0.95 Ma to 146.5 ± 1.6 Ma, strongly suggesting that the total duration of this magmatic cycle is much shorter (5.2 ± 2.6 Ma) than previously thought (~32 Ma; Ferreira and Macedo, 1983), coinciding with the Jurassic-Cretaceous transition (late Tithonian – Berrisian; Cohen et al. 2013; updated).

5.2. Magma genesis and evolution

Considering the majority of samples analysed in this study, the obtained isotopic ranges (Δ) are small ($\Delta^{87}Sr/^{86}Sr = 0.001598 \pm 0.000055$; $\Delta^{143}Nd/^{144}Nd = 0.000129 \pm 0.000026$), showing that they are representative of magmas ultimately derived from the same, practically homogeneous, source. However, three Northern samples (BL18; BL21 and BL29) present clearly higher $^{87}Sr/^{86}Sr$ ratios (up to 0.70747 vs. < 0.70606) but similar $^{143}Nd/^{144}Nd$, which is interpreted as the result of post-magmatic alteration. This will be discussed later (section 5.3), and the composition of those three samples will not be further discussed in the present section.

As shown by the TAS diagram (Fig. 4), the compositions of the studied rocks straddle the boundary between alkaline and subalkaline fields. As expected, this is also reflected by normative compositions (Fig. 7a) ranging from nepheline to quartz normative, through olivine + hypersthene normative parageneses. Interestingly this normative evolution, from SiO_2-undersaturated to SiO_2-oversaturated, inversely correlates with the Ni content (Fig. 7b) and with the Mg# of magmas but not with the isotopic compositions.

Considering these and the small range of isotopic compositions, we must conclude that crystal fractionation drove the magmas from undersaturated to oversaturated compositions, crossing the low-pressure thermal divide defined by Yoder and Tilley (1962). It has been considered that the crystallization of SiO_2-deficient minerals such as amphibole and/or spinel could induce alkaline magmas to evolve towards saturated and oversaturated compositions (e.g., Mahood and Baker, 1986; Thy and Lofgren, 1994), while experimental data obtained, for example, by Presnall et al. (1978), demonstrates that the nepheline to hypersthene normative trend can be produced by “deep” fractionation processes, occurring at pressures ranging from 0.4 to 1.2 GPa.

Despite the presence of some primary amphibole in these rocks, its occurrence is rare, which is also relatively true for the oxides, which are always a volumetrically minor component. This suggests that their fractionation did not play a major role in crossing the low-pressure thermal divide. Moreover, in Fig. 7c, the studied rocks plot close to and roughly parallel to the "high pressure" cotectic line (Sack et al., 1987), thus allowing the conclusion that the observed normative compositional evolution results from "high pressure" fractionation affecting an initially alkaline undersaturated magma.

If this model involving fractional crystallization and a reasonably homogeneous source is correct, it would be expected that, for the studied set of samples, incompatible elements with comparable and low partition coefficients (D) should vary inversely with an evolution index like Mg#. This is clearly not observed for La and Th (Fig. 8), suggesting that the studied samples represent the evolution products of magmas generated by distinct extents of melting.

This can be tested using the Zr vs. Ni diagram (Fig. 9). In such a diagram, where a highly compatible element (Ni) is plotted against a magma evolution index, as is the case of the incompatible element Zr, a fractionation process dominated by the removal of olivine and clinopyroxene, with both of which Ni is significantly compatible, would produce quasi-vertical lines, which become asymptotic with the abscissa at more advanced stages of the evolution process (see the modelled trend in Fig. 9). This is not the case for the studied rocks, which, even for slightly fractionated magmas (Ni > 100 ppm), present more than 100% relative variation of the Zr content. Considering the small range of isotopic ratios (see above), such behaviour confirms the occurrence of several melting events, characterized by distinct F (degree of partial melting) values, affecting the same source. From Fig. 9, we can infer that the Northern rocks result from the differentiation of magmas generated by higher degrees of partial melting than those

inferred from the geochemistry of the generality of the Southern rocks. For this group, the observed variability is significantly constrained by the existence of variation in the partial melting degree, while the intra-group primary variability for the Northern rocks is mainly controlled by fractional crystallization processes.

Even samples representative of only slightly evolved magmas (Ni > 100 ppm; MgO> 8 wt.%) are characterized by a significant MREE/HREE fractionation (e.g., chondrite normalized Tb/Yb ratios ranging from 1.72 to 2.39). Considering the small range of $^{143}Nd/^{144}Nd$ ratios, this can be considered as evidence for melting in the presence of residual garnet ($KD^{Yb/Tb}_{Grt/Melt} = 5.4$; $KD^{Yb/Tb}_{Cpx/Melt} = 0.9$; Mckenzie and O'Nions, 1991).

Moreover, if we also consider that $D^{Yb/Tb}_{Sp/Melt} \approx 1$, it is expected that magmas that have equilibrated with a melting residue containing garnet as the dominant Al-rich phase have higher Tb/Yb ratios than those generated in the spinel zone (e.g., George and Rogers, 2002; Wang et al., 2002; Furman et al., 2004). Assuming a primitive mantle type source composition, Wang et al. (2002) modelled the effect of the garnet-spinel transition on the magmatic Tb/Yb ratios and considered (Tb/Yb)n = 1.8 to be the threshold value separating melts generated in equilibrium with each of those minerals.

Considering that the Tb/Yb ratios cannot significantly change during the olivine/pyroxene/plagioclase-dominated fractionation processes, the positioning of our samples in Fig. 10 (i.e., Tb/Yb normalized ≥ 1.8) suggests that the magma genesis occurred on the upper part of the garnet zone, close to the transition to the spinel zone. Additionally, taking into account the small effect of fractional crystallization processes on the Th/Yb and Th/Ta ratios and considering the relatively homogeneous character of the source, implicit from the relative constancy of the Nd isotope ratios (Fig. 6) and Th/La ratios (Fig. 8), the more than 100% relative variation of the Ta/Yb ratio (Fig. 11) or more than 40% relative variation of the Tb/Yb ratio in relatively unevolved rocks

(see above) reinforces the occurrence of several episodes characterized by distinct extents of melting of a garnet-bearing source at the origin of this magmatic province.

As shown by experimental work (Robinson and Wood, 1998), the garnet-spinel transformation pressure interval is narrow (≈ 0.1 - 0.2 GPa), being centred at approximately 3 GPa (see also Klemme and O'Neill, 2000). This places the magmatic segregation in the second magmatic cycle of the Lusitanian Basin at depths slightly higher than 90 km.

5.3. Post-magmatic processes

As mentioned above, three of the studied samples are characterized by very high $^{87}Sr/^{86}Sr$ ratios (up to 0.707469) when compared with the other coeval and space-related rocks ($^{87}Sr/^{86}Sr \leq 0.7056056$). In the Sr–Nd isotopic space (Fig. 6), the studied rocks develop a quasi-horizontal trend characterized by variable $^{87}Sr/^{86}Sr$ at relatively constant $^{143}Nd/^{144}Nd$. Considering the elemental and isotopic characteristics of seawater (Steuber and Viezer, 2003; Cohen and Coe, 2007; Rickl et al., 2009) such a trend could eventually result from open-system processes directly or indirectly reflecting the composition of seawater. Indeed, the Sr-enriched elemental composition and Sr-radiogenic isotopic signature of seawater, combined with its highly Nd-depleted composition, confer upon seawater the capacity to significantly alter the $^{87}Sr/^{86}Sr$ ratios of rocks with which it interacts without any noticeable effects on the Nd isotopic signatures (see also Mourão et al., 2012).

The early Cretaceous/late Jurassic magmatic rocks, here under discussion, crop out at the onshore portion of the West Iberian Margin in intimate association with Lower Jurassic (Hettangian) sediments including clay, dolomite, limestone, and evaporites (gypsum and salt), for which we obtained chemical analyses (Table 5). From these, the

last three may be considered, to a first approximation, to be formed closely in equilibrium with seawater and, consequently, having the potential to imprint, via assimilation by basic magmas, the seawater isotopic fingerprint to the resulting rocks. This is particularly true for the evaporite materials (gypsum and rock salt), which, due to their chemical purity, should present the isotopic ratio of the water from which they precipitated. However, it should be noted that their initial Sr isotopic ratios (up to ≈ 0.70856; Table 5) are higher than those of Hettangian seawater (0.7078-0.7079; Cohen and Coe, 2007), suggesting chemical precipitation from a mixture of marine and continental waters (Alves et al., in prep.).

From the lithotypes mentioned above, only rock salt is characterized by Na_2O contents sufficiently high to increase the Na_2O concentration of the presumably contaminated rocks. However, according the results of AFC modelling, such a process also does not provide a satisfactory solution to the problem. Indeed, if based on thermal grounds, we use 0.3 as the ratio (r) between the rates of assimilation vs. fractional crystallization (e.g., DePaolo, 1981), the very low Sr concentration in rock salt (≈ 17 ppm) would imply that the amount of fractional crystallization necessary to obtain the Sr isotopic ratio of the more radiogenic basaltic rock would represent more than 95% of the initial mass of the magmatic liquid. Considering the weakly evolved composition of the most Sr-radiogenic rock (e.g., Mg# = 54; Ni > 40 ppm) such an amount of crystallization is clearly inadequate. The same conclusion would also emerge if r = 0.8 is used, given the dramatic effects on the major element composition, or considering the energy-constrained assimilation-fractional crystallization (EC-AFC) model of Bohrson and Spera (2001).

The increase of $^{87}Sr/^{86}Sr$ at a relatively constant $^{143}Nd/^{144}Nd$ is consentaneous with rock-seawater chemical interaction, a common process in situations of magma extrusion

in submarine environments (Kawahata et al. 1987; Mourão et al. 2012). However, the studied rocks are intrusive and do not show any of the morphological aspects typically assigned to submarine magmatism (e.g., pillow structures), thus allowing an alternative explanation. This involves the post-magmatic hydrothermal alteration of basaltic rocks by brines, resulting from the interaction of circulating meteoric water with the neighbouring saline sediments. This process would explain the fact that the most Sr-radiogenic samples are those characterized by a higher LOI. Also explained by this process is the evident hydrothermal alteration of the basaltic rocks (see 4.2), particularly obvious in the most Sr-radiogenic rocks, as well as the very large dispersion observed in diagrams involving large ion lithophile incompatible elements such as Ba and Cs (Fig. 12), as opposed to what is observed in plots involving only high field strength elements (Fig. 8). Additionally, such a process would cause a sodium increase, with the Na_2O contents tending to be higher at the most Sr radiogenic samples (see 4.4). This leads to the occurrence of normative nepheline in rocks, which deviates significantly from the broad negative correlation between the Ni content (a proxy for the magma evolution degree) and the degree of silica saturation (Fig. 7b).

5.4 Considerations on the second cycle mantle source within the framework of the WIM geodynamics

As shown above (section 5.1), igneous occurrences associated with the second onshore Mesozoic magmatic cycle in the WIM are restricted to the Lusitanian Basin (LB) and to a short period between circa 148 and 140 Ma, coincident with the Jurassic-Cretaceous transition. According to Grange et al. (2008), these mildly alkaline rocks represent the oldest rift-related magmatism associated with the Iberia-Newfoundland split-up, predating by ≈ 15 Ma the Newfoundland offshore alkaline magmatism previously

considered by Jagoutz et al. (2007) as the precursor of what they call the embryonic seafloor spreading.

The presence of magnetic anomalies back to M20 at the WIM and at the conjugated Newfoundland margin (Srivastava et al., 2000; Sibuet et al., 2007) arguably dates the initiation of the ocean floor spreading at circa 146 Ma ago (see also Seton et al., 2012; cf. Bronner et al., 2011; Minshull et al. 2014), i.e., at the times of the emplacement of the onshore second magmatic cycle. This was followed by the genesis of the remarkable lithospheric peridotite ridge emplaced at the ocean-continent transition, along Northwestern Iberia (Fig. 1), which was intruded by gabbros and locally capped by basalts/dolerites, with both depleted and enriched isotopic signatures. Indeed, while some of these rocks are enriched relative to N-MORB (e.g., εNd_i down to 2.2; Seifert et al., 1996; Seifert and Brunotte, 1996; Charpentier et al., 1998; Cornen et al., 1999), other are highly depleted, such as the 138-136 Ma gabbros at the Gorringe Bank (εHf_i up to + 20.5 ± 0.3; Scharer et al., 2000) and the 136.4 Ma gabbros at the Iberia Abyssal Plain (εNd_i up to +10.3; Seifert et al., 1996).

These depleted magmatic rock occurrences were interpreted as evidence either for a magmatically active mid-ocean ridge in the Iberia Abyssal Plain during the Early Cretaceous (Seifert et al., 1996) or of syn-rift asthenospheric magmatism immediately preceding the continental breakup (Scharer et al., 2000).

On the other hand, the relatively enriched geochemical signatures were viewed as indicating a plume contribution, which points to a plume-induced rifting process (Seifert and Brunotte, 1996). However, plume magmatism is usually voluminous and preceded by uplift (e.g., Ernst and Buchan, 2003), which is not the case at the WIM, as recognized by those authors, invalidating this model, in our opinion. Nevertheless, the existence of passive ancient plume material derived from stagnated weak plumes

beneath old and thick lithospheres has been suggested (Stein and Hofmann, 1994; Ernst and Buchan, 2003). In this perspective, the existence in the asthenosphere of enriched fossil plume domains, later remobilized during extension, could be hypothesized as an explanation for the relatively enriched character of some of the Lower Cretaceous magmatism. A different point of view was defended by Charpentier et al. (1998) and Chazot et al. (2005), who considered such enriched signatures in the off-shore rocks as resulting from the mixing of ascending depleted asthenospheric magmas with enriched lithospheric melts.

The slight delay of the second onshore magmatic cycle (148 to 140 Ma) with respect to the Late Jurassic rifting event (from the Oxfordian to the Berriasian; e.g., Wilson et al., 1989; Rasmussen et al., 1998; Alves et al., 2006; Dinis et al., 2008; Pereira and Alves, 2011; Kullberg et al., 2013), which was accompanied by important tectonic subsidence, salt diapirism and rift shoulder uplift, point to a link between these two events, suggesting a passive-type model where magmatism is induced by tensional stresses generated in the continental lithosphere (e.g., Geoffroy, 2005) rather than being plume-related, which would be preceded by domal uplift, shoaling and offlapping in the regional sedimentation (e.g., Ernst and Buchan, 2003).

For the second onshore magmatic cycle, Grange et al. (2008) proposed a lithospheric origin for magmas, mainly based on somewhat radiogenic Sr isotope signatures (initial $^{87}Sr/^{86}Sr = 0.70646$) and on high $^{207}Pb/^{204}Pb$ for a given $^{206}Pb/^{204}Pb$ determined for one of the studied samples. We did not analyse lead isotopes. However, we demonstrated before that samples with $(^{87}Sr/^{86}Sr)_i > 0.7052$, characterized by a high $^{87}Sr/^{86}Sr$ for a given $^{143}Nd/^{144}Nd$ and by high Na_2O contents (up to 5.66 wt%), provide evidence for exogenous processes involving Jurassic saline materials. This recommends caution on the use of Sr isotopes in these rocks and recommends a re-evaluation of the model

proposed by Grange et al. (2008), inasmuch as the referred initial $^{207}Pb/^{204}Pb$ ratio (15.925) is clearly higher than that of the typical subcontinental lithospheric mantle (see, for example, Fig. 6a from Grange et al., 2008).

Above, based on the $(Tb/Yb)_n$ ratios, we considered that the magma genesis responsible for the rocks studied here would have occurred at the top of the garnet lherzolite zone corresponding to depths slightly deeper than 90 km. Considering that the estimated lithosphere thickness for the region exceeds 120 km (Tesauro et al., 2013; see also Férnandez et al., 1998), our data clearly support a lithospheric origin for the magmas, as previously proposed by Grange et al. (2008). Data presented by Scharer et al. (2000) and Chazot et al. (2005) for off-shore magmatic rocks slightly younger than those onshore reveal that they are characterized by similar or lower MREE/HREE ratios. This suggests that part of the Early Cretaceous offshore rocks could have been generated in the spinel zone, thus probably also having a lithospheric origin.

A lithospheric origin for the studied magmas is also supported by the comparison of the unaltered rock compositions studied here ($^{143}Nd/^{144}Nd$ from 0.512686 to 0.512800; $^{87}Sr/^{86}Sr$ from 0.704458 to 0.705268) with those determined by Chazot et al. (2005) for clinopyroxenes in the Iberia Abyssal Plain websterites ($^{143}Nd/^{144}Nd$ from 0.512283 to 0.512553; $^{87}Sr/^{86}Sr$ from 0.704170 to 0.705919). Indeed, these were interpreted as samples of the metasomatized sub-continental lithosphere, and their Sr-radiogenic and Nd-unradiogenic signatures support, in our opinion, a model invoking the metasomatized continental lithosphere as the magma source, given that refertilized lithospheric domains are considered prone to act as sources of magma (e.g., France et al., 2015). From this perspective, the somewhat more silica-undersaturated characteristics and enriched signatures of the onshore magmas (εNd_i down to +1.6), when compared with the quasi-coeval offshore magmas (εNd_i down to +2.2), could be

interpreted as a consequence of the off-rift axis positioning of the studied onshore region. This implies a comparatively smaller onshore lithospheric stretching, which would have restricted the extent of partial melting, allowing the preferential sampling of the more enriched/lower solidus lithospheric portions generated by previous metasomatic events (see, for example, Martins et al., 2010; France et al., 2015).

5.5 The role of Variscan fractures reactivation

The studied rocks mainly occur as dykes, sills, and other small intrusions, thus representing an upper crustal plumbing system(s), exhumed and presently exposed by erosion.

It is accepted that, at least at high crustal levels, the magma migration/ascent towards the Earth's surface dominantly proceeds through hydraulic fracturing, causing dyke propagation (e.g., Taisne and Jaupart, 2011), or using pre-existing fracture systems, which may control the ascent path and the local magma emplacement/extrusion. Most of the onshore second cycle igneous outcrops occur along Mesozoic NNE-SSW striking rift faults such as the Porto de Mós – Rio Maior fault (Fig. 2), one of many inherited Variscan basement faults initially formed during the Permian (Arthaud and Matte, 1975, 1977). This shows that the main syn-rift NNE-SSW striking faults, which accommodate most of the Late Jurassic-Earliest Cretaceous tectonic extension, propagated to the depth of existing magma chambers, thus playing an active role in the ascent and distribution of the second magmatic cycle rocks in the LB. These faults also served as conduits for the ascent of salt walls across the whole 3-4 km thick Jurassic sequence and were reactivated during the Cenozoic tectonic inversion (e.g., Ribeiro et al., 1990).

The ENE-WSW striking Nazaré Fault is also an inherited Variscan Fault that subdivides the LB into two main blocks with different stratigraphic records (e.g., Wilson et al.,

1998; Kullberg et al., 2013; Pena dos Reis et al., 2011). Additionally, different subsidence histories and stretching coefficients for the northern and southern parts of the LB across the Nazaré Fault were found based on backstripping analysis and apatite fission track studies (Stapel et al., 1996). For these authors, such differences suggest different crustal thicknesses or densities across the Nazaré Fault, implying a thinner or denser crust in the Southern block, which, according to Tesauro et al. (2013), is characterized by a thinner lithosphere and higher heat flow.

The geochemical contrast reported in this work between rocks cropping out to the north and south of the Nazaré fault, with the Southern rocks being clearly less evolved ($58.81 \leq Mg\# \leq 67.43$; $77 \leq Ni \leq 214$ ppm) than those from the Northern sector ($33.17 \leq Mg\# \leq 56.13$; $2 \leq Ni \leq 101$ ppm), strongly suggests that such variability of the LB basement played a role in the magma differentiation. Moreover, the observed distinct granularities (Northern rocks are coarser; see section 4.1) points to different depths of final magma emplacement.

After generation, mafic magmas are less dense than melting residues and sources, being positively buoyant. Consequently, they tend to migrate upwards in the mantle and crust to a depth where they eventually stagnate and differentiate. The depth of crustal magma trapping has been considered dependent of the existence of a neutral-buoyancy level (NBL) (Glazner and Ussler III, 1998; Ryan, 1994). However, Jagoutz (2014), emphasizing that at continental arcs there is no evidence for the existence of such NBLs, suggested that melt stagnation is mainly dominated by temperature.

Despite the fact that the studied rocks are intrusive, they do not show evidence of significant crystal accumulation, and their compositions can be considered as representative of magmatic liquids. Considering the similar primary magma compositions (i.e., temperatures, see section 5.2) in both the South and North Nazaré

Fault sectors, the different magma evolution degrees and depths of emplacement probably resulted from the different thermal regimes in the crustal blocks separated by the Nazaré Fault. The more evolved composition of the Northern rocks suggests the existence of more important magma chambers (s.l.) in this domain, with respect to the Southern sector, where the majority of magmas reach their local final emplacement site without suffering significant differentiation, i.e., without significant stalling at deeper crustal levels. Indeed, the lower geothermal gradient inferred for the Northern sector (Tesauro et al., 2013) implies that the ascending Northern magmas crossed the *liquidus* at deeper crustal levels and probably stagnated in depth because significant crystallization occurs over a small temperature interval (e.g., Jagoutz, 2014). This would have favoured the genesis of reservoirs where the magmas fractionated before their evolved fractions migrate to higher crustal levels using the inherited Variscan fractures (see above).

It is worthwhile to note a striking difference in the tectonic control of dyke emplacement during the second and third magmatic cycles in the WIM. The second cycle (late- to syn-rift) dykes intruded mainly along syn-rift faults, while the third cycle (post-rift) dykes do not show any extensional control. As examples, we refer to the radial dyke complex around the Late Cretaceous Mafra intrusion and a W-E 350 km long dyke corridor (N 39º 50') striking across the WIM just south of the study area (Neres et al., 2014). As proposed by these authors, these dykes used W-E striking faults parallel to the oceanic transform faults that separated previously extended blocks during rifting and oceanic break up.

5.6 The onshore magmatic evolution of the WIM

The most important characteristic of the WIM is its magma-poor nature, with a significant width of the transition zone between the oceanic and continental crust and also the presence of exhumed mantle blocks (e.g., Pinheiro et al., 1996; Whitmarsh et al., 2001; Jagoutz et al., 2007; Reston et al., 2009; Bronner et al., 2011; Minshull et al. 2014). These characteristics are somewhat contrasting with those of the Central and Southern Atlantic (e.g., Moulin et al., 2010) and can be interpreted as resulting from lower extension rates caused by a closer proximity of Iberia to the Euler rotation pole during the North Atlantic opening (Ludin et al., 2014). We interpret this smaller extension as the cause for the two long hiatuses in the magmatic activity at the onshore WIM. Indeed, the onshore evolution of the WIM was marked by the occurrence of three magmatic cycles (202 to 198 Ma; 148 to 140 Ma; 94 to 69 Ma) separated by periods of circa 50 Ma of magmatic quiescence (Rapaille et al., 2003; Verati et al., 2007; Miranda et al., 2009; Grange et al., 2008; Grange et al., 2010; this study).

As shown by Figs. 4, 6 and 10, magmatism evolved from tholeiitic (1st cycle) to alkaline (3rd cycle) through mildly alkaline (2nd cycle) affinities. Magmas become, with time, more enriched in incompatible elements, while their sources were progressively characterized by a more marked time-integrated depletion, as depicted by an evolution to lower $^{87}Sr/^{86}Sr$ but higher $^{143}Nd/^{144}Nd$ ratios (Fig. 6; see also Mata et al., 2011). A change with the time in the depth of magma segregation is also evident from Fig. 10, where a progressive increase is deduced from the Tb/Yb ratios.

These characteristics could eventually suggest a model explaining the variability of the WIM onshore Mesozoic magmatism by different degrees of plume-lithosphere interaction. In such a hypothesis, the second magmatic cycle, here studied, presents compositions intermediate between those of the first cycle (lithosphere originated; e.g.,

Martins et al., 2008) and those of the third cycle (plume-derived; Grange et al., 2010), which would result from the mixing of plume- and lithosphere-derived magmas. From Fig. 13, it can be concluded that the second cycle rocks plot on a hypothetical mixing line between the compositions of the first and third magmatic cycles. However, there is much geological evidence that does not support such a model.

First, it is difficult to conciliate the positioning of the LB region above a mantle plume for more than 70 Ma (from 148 to 69 Ma) with a volcanic hiatus of circa 50 Ma, which is not usually observed at plume-related magmatic provinces. Moreover, the second magmatic cycle was shortly preceded and coeval with a rifting event accompanied by important tectonic subsidence and sedimentation, which is not compatible with the role of a mantle plume. Instead, magma genesis must have occurred in the sub-continental lithosphere mantle (Grange et al., 2008; this paper section 5.4), induced by tensional stresses (passive-type rifting). A similar situation characterized the evolution of the South Iberian Margin and Northwest Africa, where it has been shown that the tholeiitic 1st cycle was preceded by subsidence and sedimentation (e.g., Martins et al., 2008; Uphoff, 2005).

1-D backstripping and subsidence analyses, performed by Cunha (2008) using onshore borehole data, clearly demonstrate that the WIM extension was more significant during the Triassic-early Jurassic rifting episode than during subsequent rifting episodes (see also Stapel et al., 1996; Teixeira et al., 2012) which, through the implicitly larger degrees of partial melting (e.g., McKenzie and Bickle, 1988; Ellam, 1992), partially explains the tholeiitic signatures of the 1st cycle rocks as opposed to the mildly alkaline characteristics of the 2nd cycle rocks. However, taking into account that the Sr and Nd isotope signatures are not modified during partial melting events, the differences depicted by Fig. 6 clearly indicate that the magmas erupted during those two cycles

were generated from distinct sources, with the one feeding the second cycle characterized by higher time-integrated Rb/Sr but lower Sm/Nd ratios.

In the Upper Cretaceous, during which the third onshore WIM magmatic cycle occurred (e.g., Rock, 1982; Miranda et al., 2009), no lithospheric stretching can be inferred from the backstripping analyses, nor from inspection of the seismic reflection data or field geology (e.g., Rasmussen et al., 1998; Terrinha et al., 2003). In this context, lithospheric stretching does not offer a plausible explanation for the generation of magma volumes capable of justifying the Upper Cretaceous Lisbon Volcanic Complex, the Sintra, Sines and Monchique intrusive massifs and other minor occurrences. This confers plausibility to plume models such as those proposed by Merle et al. (2009) and Grange et al. (2010), and also alternatively suggested by Miranda et al. (2009), to explain the occurrence of the third WIM magmatic cycle.

Rocks from this third cycle are characterized by high silica under-saturation and significant enrichment in incompatible trace elements. These and the high depth of magma segregation reflect the lid effect (see Watson and Mckenzie, 1991; Niu et al., 2011) of a probably already thickened lithosphere as a result of post-rift mechanical/thermal recovery (Leroy et al., 2008). The lid impeding the plume ascent constrained the top of the melting column generated by adiabatic plume decompression and, as a consequence, limited the extent of partial melting.

In conclusion, the WIM Mesozoic onshore magmatism, spanning in time for some 130 Ma, reflects the main phases of the development of Mesozoic peri-Iberian basins since its inception in the Triassic until the Upper Cretaceous, when drift between Iberia and Newfoundland was already established. It testifies to magma transfer processes from the sub-WIM mantle lithosphere to the crust during periods comprising rifting processes associated with the initial stages of the Atlantic opening (immediately predating the 1st

and 2nd cycles) and the role of a mantle plume during the passive margin stage (3rd cycle).

6. Concluding Remarks

- The second onshore Mesozoic magmatic cycle at the West Iberian Margin (WIM) span in time from, at least, 148 to 140 Ma, having produced mildly alkaline magmas that evolved at relatively high pressure (≥ 8 kb) to SiO_2-saturated and -oversaturated compositions.
- The magmatism was most probably generated in the lithosphere and preceded by an important extensional event that is interpreted as a consequence of the lithospheric thinning related to the Atlantic opening.
- The magma emplacement was controlled by rift faults that resulted from the reactivation of late orogenic Permian strike-slip faults, which also controlled the location of the associated salt walls.
- Rocks emplaced north of the Nazaré Fault are clearly more evolved than their southern counterparts, which point to more voluminous and deeper magma chambers in the Northern sector. This is interpreted as indicating different temperature profiles for those sectors.
- The Northern rocks are the result of the differentiation of magmas generated by higher degrees of partial melting than those inferred from the geochemistry of the generality of the Southern rocks, whose variability reflects the existence of several distinct events of partial melting.
- Part of the variability of the studied magmatic rocks is due to their hydrothermal alteration involving brines formed by the interaction of meteoric water with the neighbouring Lower Jurassic evaporitic rocks. These effects are more visible for

Northern rocks, producing significant increases in the Na_2O contents and $^{87}Sr/^{86}Sr$ ratios.

Acknowledgements

This project was mainly supported by FCT through projects PEST-OE/CTE/UI0263/2011-2013 (Centro de Geologia da Universidade de Lisboa) and PEST-OE/CTE/LA0019/2013-2014 (Instituto Dom Luiz - UID/GEO/50019/2013). We acknowledge financial support from the Petrobras/GALP/Partex consortium through an agreement signed with the Universidade de Lisboa as a counterpart for offshore exploration activities in Portugal (2008-2013). Additional support was provided by CNRI (Italy), CNRST (Morocco) and FCT (Portugal) through bilateral cooperation projects and also by the CAT project. We are indebted to Sara Ribeiro for keeping at top running condition the Laboratório de Análises Isotópicas da Universidade de Aveiro, where the Sr and Nd analyses were performed, and Pedro Rodrigues for the performing of the EMP analyses. Editorial handling by Nelson Eby and constructive reviews by Renaud Merle and Olivier Jagoutz are also acknowledged.

References

Adam, J., Green, T., 2006. Trace element partitioning between mica- and amphibole-bearing garnet lherzolite and hydrous basanitic melt: 1. Experimental results and the investigation of controls on partitioning behavior. Contributions to Mineralogy and Petrology 152, 1-17.

Afilhado, A., Matias, L., Shiobara, H., Hirn, A., Mendes-Victor, L., Shimamura, H., 2008. From unthinned continent to ocean: The deep structure of the West Iberia passive continental margin at 38ºN. Tectonophysics, 458, 9-50.

Alves, C.A.M., Rodrigues, B., Serralheiro, A., Faria, A.F.P., 1980. O complexo basáltico de Lisboa. Comunicações dos Serviços Geológicos de Portugal 66, 111-134.

Alves, T.M., Moita, C., Sandnes, F., Cunha, T., Monteiro, J.H., Pinheiro, L.M., 2006. Mesozoic-Cenozoic evolution of North Atlantic continental-slope basins: the Peniche Basin, western Iberian margin. American Association of Petroleum Geologists Bulletin 90, 31-60.

Alves, T.M., Moita, C., Cunha, T., Ullnaess, M., Mycklebust, R., Monteiro, J.H., Manupella, G., 2009. Diachronous evolution of Late Jurassic-Cretaceous continental rifting in the North Atlantic (West Iberian margin). Tectonics 28(4), TC4003, doi: 10.1029/2008TC002337.

Arthaud, F. and Matte, P., 1975. Les decrochements tardi-hercyniens du sud-ouest de l'europe. Geometrie et essai de reconstitution des conditions de la deformation, Tectonophysics, 25, 139-171.

Arthaud, F. and Matte, P., 1977. Late Paleozoic strike-slip faulting in Southern Europe and Northern Africa: result of a right-lateral shear zone between the Appalachians and the Urals, Geological Society of America Bulletin, 88, 1305-1320.

Azerêdo, A.C., Wright, V.P., Ramalho, M.M., 2002. The Middle-Late Jurassic forced regression and disconformity in Central Portugal: eustatic, tectonic and climatic effects on a carbonate ramp system. Sedimentology 49, 1339-1370.

Baksi, A.K., 2006. Guidelines for assessing the reliability of $^{40}Ar/^{39}Ar$ plateau ages: application to ages relevant to hotspot tracks. http://www.mantleplumes.org/ArAr

Beslier, M.-O., Cornen, G., Girardeau, J., 1996. Tectonometamorphic evolution of peridotites from ocean-continent transition of the Iberia Abissal Plain Margin. In: Withmarsh, R.B., Sawyer, D.S., Klaus, A., Masson, D.G., (Eds), Proceedings of the Ocean Drilling Program, Scienttific Results, Vol 149, 397-412.

Bohrson, W.A., Spera, F.J., 2001. Energy-Constrained Open-System Magmatic Processes II: Application of Energy-Constrained Assimilation-Fractional Crystallization (EC-AFC) Model to Magmatic Systems. Journal of Petrology 42, 1019-1041.

Bronner, A., Sauter, D., Manatschal, G., Péron-Pinvidic, G., Munschy, M., 2011. Magmatic breakup as an explanation for magnetic anomalies at magma-poor rifted margins. Nature Geosciences 4, 549-553.

Callegaro, S., Rapaille, C., Marzoli, A., Bertrand, H., Chiaradia, M., Reinsberg, L., Bellieni, G., Martins, L., Madeira, J., Mata, J., Youbi, N., De Min, A., Azevedo, M.R., Bensalah, M.K., 2014. Enriched mantle source for the Central Atlantic magmatic province: new supporting evidence from southwest Europe. Lithos 188, 15-32.

Carvalho, J., Matias, H., Torres, L., Manupella, G., Pereira, R., Mendes-Victor, L., 2005. The structural and sedimentary evolution of the Arruda and Lower Tagus sub-basins, Portugal. Marine and Petroleum Geology 22, 427-453.

Cebriá, J.M., Lopez-Ruiz, J., Doblas, M., Martins, L.T., Munhá, J., 2003. Geochemistry of the Early Jurassic Messejana-Plasencia dyke (Portugal-Spain): implications on the origin of the Central Atlantic Magmatic Province. Journal of Petrology 44, 547-568.

Charpentier, S., Kornprobst, J., Chazot, G., Cornen G. et Boillot G., 1998. Interaction entre lithosphère et asthénosphère au cours de I'ouverture océanique: dormées isotopiques préliminaires sur la Marge passive de Galice (Atlantique-Nord). Comptes Rendus de l' Academie des Sciences de Paris, Sciences de la Terre et des Planètes, 326, 757-762.

Chazot, G., Charpentier, S., Kornprobst, J., Vannucci, R., Luais, B., 2005. Lithospheric mantle evolution during continental break-up: the West Iberia non-volcanic passive margin. Journal of Petrology 46, 2527-2568.

Cohen, A.S., Coe, A.L., 2007. The impact of the Central Atlantic Magmatic Province on climate and on the Sr- and Os-isotope evolution of seawater. Palaeogeography, Palaeoclimatology, Palaeoecology 244, 374-390.

Cohen, K.M., Finney, S.C., Gibbard, P.L., Fan, J.-X. (2013; updated) The ICS International Chronostratigraphic Chart. Episodes 36: 199-204.

Cornen, G., Girardeau, J., Monnier, C., 1999. Basalts, underplated gabbros and pyroxenites record the rifting process in the West Iberian margin. Mineralogy and Petrology 67, 111-142.

Cunha, T., 2008. Gravity anomalies, flexure and the thermal and mechanical evolution of the West Iberian Margin and its conjugate of Newfoundland. PhD Thesis, Department of Earth Sciences, Oxford University.

DePaolo, D.J., 1981. Trace elements and isotopic effects of combined wallrock and fractional crystallization. Earth and Planetary Science Letters, 53, 189-202.

DePaolo, D. J., 1988. Neodymium isotope geochemistry, an introduction. Springer-Verlag, Berlin.

Dinis, J.L., Rey, J., Cunha, P.P., Callapez, P., 2008. Stratigraphy and allogenic controls of the western Portugal Cretaceous: an updated synthesis. Cretaceous Research 29, 772–780.

Duarte, L.V., Silva, R.L., Mendonça Filho, J.G., Poças Ribeiro, N., Chagas, R.B.A., 2012. High-resolution stratigraphy, palynofacies and source rock potential of the Água de Madeiros Formation (Lower Jurassic), Lusitanian Basin, Portugal. Journal of Petroleum Geology 35, 105-126.

Duncan, R., Keller, R., 2004. Radiometric ages for basement rocks from the Emperor Seamounts, ODP Leg197. Geochemistry, Geophysics, Geosystems 5(8), Q08L03, doi: 10.1029/2004GC000704

Ellam, R.M., 1992. Lithospheric thickness as a control on basalt geochemistry. Geology 20, 153-156.

Ernst, E., Buchan, K., 2003. Recognizing mantle plumes in the geological record. Annual Review of Earth and Planetary Sciences 31, 469-523.

Fernàndez, M., Marzám, I., Correia, A., Ramalho, E., 1998. Heat flow, heat production, and lithospheric thermal regime in the Iberian Peninsula. Tectonophysics 291, 29–53.

Ferreira, M.P., Macedo, C.R., 1983. Igneous rocks in the diapiric areas of the western Portuguese border: the K-Ar ages and settings of the Upper Jurassic suite. Memórias e Notícias da Universidade de Coimbra 96, 159-181.

Fleck, R. J., Sutter, J. F., Elliot, D. H., 1997. Interpretation of discordant $^{40}Ar/^{39}$ Ar age spectra of Mesozoic tholeiites from Antarctica. Geochimica et Cosmochimica Acta 41, 15 - 32

France, L., Chazot, G., Kornprobst, J., Dallai, L., Vannucci, R., Gregoire, M., Bertrand, H., Boivan, P., 2015. Mantle refertilization and magmatism in old orogenic regions: The role of late-orogenic pyroxenites. Lithos (2015) doi: 10.1016/j.lithos.2015.05.017.

Furman, T., Bryce, J., Karson, J., Iotti, A., 2004. East African rift system (EARS) plume structure: insights from Quaternary mafic lavas of Turkana, Kenya. Journal of Petrology 45, 1069-1088.

Geoffroy, L., 2005. Volcanic passive margins. Comptes Rendus Geoscience 337, 1395 1408.

George, R.M., Rogers, N.W., 2002. Plume dynamics beneath the African Plate inferred from the geochemistry of the tertiary basalts of southern Ethiopia. Contributions to Mineralogy and Petrology 144, 286-304.

Glazner, A.F.,Ussler III,W.,1988. Trapping of magma at mid crustal density discontinuities. Geophysical Research Letters 15, 673–675.

Grange, M., Scharer, U., Comen, G., Girardeau, J., 2008. First alkaline magmatism during Ibéria – Newfoundland rifting. Terra Nova 20, 494-503.

Grange, M., Scharer, U., Merle, R., Girardeau, J., Comen, G., 2010. Plume-Lithosphere interaction during migration of Cretaceous alkaline magmatism in SW Portugal: evidence from U-Pb ages and Pb-Sr-Hf isotopes. Journal of Petrology 51, 1143-1170.

Green, T.H., Pearson, N.J., 1987. An experimental study of Nb and Ta partitioning between Ti-rich minerals and silicate liquids at high pressure and temperature. Geochimica et Cosmochimica Acta 51, 55-62

Irvine, T.M., Baragar, W.R.A., 1971. A guide to the chemical classification of the common volcanic rocks. Canadian Journal of Earth Sciences 8, 523-548.

Jagoutz, O., Munstener, O., Manatschal, G., Rubatt, D., Péron-Pinvidic, G., Brent, D.T., Villa, I., 2007. The rift-to-drift transition in the North Atlantic: a stuttering start of the MORB machine? Geology 35, 1087-1090.

Jagoutz, O., 2014. Arc crustal differentiation mechanisms. Earth and Planetary Science Letters 396, 267-277.

Kawahata, H., Kusakabe, M., Kikuchi, Y., 1987. Strontium, oxygen and hydrogen isotope geochemistry of hydrothermally altered and weathered rocks in DSDP Hole 504B, Costa Rica Rift. Earth and Planetary Science Letters 85, 343-355.

Klemme, S., O'Neill, H., 2000. The near solidus transition from garnet lherzolite to spinel lherzolite. Contributions to Mineralogy and Petrology 138, 237-248.

Koppers, A.A.P., 2002. ArArCALC – software for $^{40}Ar/^{39}Ar$ age calculations. Computers and Geosciences 28, 605-619.

Kullberg, J.C., Rocha, R.B., Soares, A.F., Rey, J., Terrinha, P., Azerêdo, A.C., Callapez, P., Duarte, L.V., Kullberg, M.C., Martins, L., Miranda, R., Alves, C., Mata, J., Madeira, J., Mateus, O., Moreira, M., Nogueira, C.R., 2013. A Bacia Lusitaniana: Estratigrafia, Paleogeografia e Tectónica, in: Dias, R., Araújo, A., Terrinha, P., Kullberg, J.C. (Eds), Geologia de Portugal, Escolar Editora, Lisboa, Vol. 2, pp. 195-347. ISBN 978-972-592-364-1

LeBas, M.J., LeMaitre, R.W., Streckeisen, A., Zanettin, B., 1986. A chemical classification of volcanic rocks based on the total alcali-silica diagram. Journal of Petrology 27, 745-750.

Laboratório Nacional de Energia e Geologia, 2010. Carta Geológica de Portugal à escala 1:1 000 000. Laboratório Nacional de Energia e Geologia, Laboratório de Geologia e Minas, Lisboa.

Ludin, E.R., Redfield, T.F., Péron-Pinvidic, G., 2014. Rifted continental margins: geometric influence on crustal architecture and melting, in: Pindell, J., Horn, B., Rosen, N., Weimer, P., Dinkleman, M., Lowrie, A., Fillon, R., Granath, J., Kennien, L. (Eds), Sedimentary basins: origin, depositional histories and petroleum systems, 33rd Annual GCSSEPM Foundation Bob F. Perkins Research Conference, pp. 18-53.

Leroy, M., Gueydan, F., Danteuil, O., 2008. Uplift and strength evolution of passive margins inferred from 2-D condutive modelling. Geophysics Journal International 172, 464-476.

Mahood, G., Baker, D.R., 1986. Experimental constraints on depths of fractionation of mildly alkalic basalts and associated felsic rocks: Pantelleria, Strait of Sicily. Contributions to Mineralogy and Petrology 93, 251-264.

Martins, L.T., 1991. Actividade Ígnea Mesozóica em Portugal (Contribuição Petrológica e Geoquímica). PhD Thesis, University of Lisbon, 418 pp.

Martins, L.T., 1999. Cretaceous alkaline magmatism in the Algarve littoral (South Portugal): a basanite-lamprophyre suite. Geolines 9, 84-91.

Martins, L.T., Madeira, J., Youbi, N., Munhá, J., Mata, J., Kerrich, R., 2008. Rift-related magmatism of the Central Atlantic magmatic province in Algarve, Southern Portugal. Lithos 101, 102-124.

Martins, S., Mata, J., Munhá, J., Mendes, M.H., Maerschalk, C., Caldeira, R., Mattielli, N., 2010. Chemical and mineralogical evidence of the occurrence of mantle metasomatism by carbonate-rich melts in an oceanic environment (Santiago Island, Cape Verde). Mineralogy and Petrology 99, 43-65.

Marzoli, A., Renne, P.R., Piccirillo, E.M., Ernesto, M., Bellieni, G., DeMin, A., 1999. Extensive 200-million-year-old continental flood basalts of the Central Atlantic Magmatic Province. Science 284, 616-618.

Mata, J., Munhá, J., 2004. Madeira Island alkaline lava spinels: petrogenetic implications. Mineralogy and Petrology 81, 85-111.

Mata, J., Alves, C. F., Miranda, R., Martins, L., Madeira, J., Terrinha, P., Youbi, N., Bensalah, M.K., Azevedo, M.R., 2011. The Mesozoic evolution of the West Iberian Margin as witnessed by magma geochemistry. 2011 Goldschmidt Conference (Prague). Mineralogical Magazine 75, 1423.

McDonough, W.F., Sun, S.-s., 1995. The composition of the Earth. Chemical Geology 120, 223-253.

McKenzie, D., Bickle, M.J., 1988. The volume and composition of melt generated by extension of lithosphere. Journal of Petrology 29, 625-679.

McKenzie, D., O'Nions, R.K., 1991. Partial melt distributions from inversion of rare earth element concentrations. Journal of Petrology 32, 1021-1091.

Merle, R., Schärer, U., Cornen, G., Girardeau, J., 2006. Cretaceous seamounts along the continent-ocean transition of the Iberian Margin: U–Pb ages and Pb–Sr–Hf isotopes. Geochimica et Cosmochimica Acta 70, 4950–4976.

Merle, R., Jourdan, F., Marzoli, A., Renne, P.R., Grange, M., Girardeau, J., 2009. Evidence of multi-phase Cretaceous to Quaternary alkaline magmatism on Tore–Madeira Rise and neighbouring seamounts from $^{40}Ar/^{39}Ar$ ages. Journal of the Geological Society 166, 879–894.

Middlemost, E.A.K., 1989. Iron oxidation ratios, norms and the classification of volcanic rocks. Chemical Geology 77, 19-26.

Min, K.W., Mundil, R., Renne, P.R., Ludwig, K.R., 2000. A test for systematic errors in $^{40}Ar/^{39}Ar$ geochronology through comparison with U/Pb analysis of a 1.1-Ga rhyolite. Geochimica et Cosmochimica Acta 64, 73-98.

Minshull, T.A., Dean, S.M. and Whitmarsh, R.B. (2014) The peridotite ridge province in the southern Iberia Abyssal Plain: seismic constraints revisited. Journal of Geophysical Research 119, 1580-1598.

Miranda, R., Valadares, V., Terrinha, P., Mata, J., Azevedo, M.R., Gaspar, M., Kullberg, J.C., Ribeiro, C., 2009. Age constraints on the Late Cretaceous alkaline magmatism on the West Iberian Margin. Cretaceous Research 30, 575-586.

Miranda, R., 2010. Petrogenesis and geochemistry of the Late Cretaceous alkaline magmatism in the West Iberian Margin. PhD thesis, University of Lisbon, 366 pp.

Morais, J.C., Neiva, J.M., 1947. Rochas eruptivas dos domos eruptivos de S. Bartolomeu, Monte Redondo e Pinhal Real, Distrito de Leiria. Revista da Faculdade de Ciências de Coimbra XVI, 5-25.

Moulin, M., Aslanian, D., Unternehr, P., 2010. A new starting point for the South and Equatorial Atlantic Ocean. Earth-Science Reviews 98, 1–37.

Mourão, C., Mata, J., Doucelance, R., Madeira, J., Millet, M.-A., Moreira, M., 2012. Geochemical temporal evolution of Brava Island magmatism: constraints on the variability of Cape Verde mantle sources and on the carbonatite-silicate magma link. Chemical Geology 334, 44-61.

Neres, M.,. Bouchez, J.L. Terrinha, P., Font, E., Moreira, M., Miranda, R., Launeau, P., Carvalho C., 2014. Magnetic fabric in a Cretaceous sill (Foz da Fonte, Portugal): flow model and implications for regional magmatism. Geophysical Journal International 199, 78–101.

Niu, Y., Wilson, M., Humphreys, E.R., O'Hara, M.J., 2011. The origin of intra-plate Ocean Island Basalts (OIB): the lid effect and its geodynamic implications. Journal of Petrology 52, 1443-1468.

Ozima, M., Podosek, F.A., 2002. Noble gas geochemistry, Cambridge University Press, 286 pp.

Paster, T.P., Schauwecker, D.S., Haskin, L.A., 1974. The behavior of some trace elements during solidification of the Skaergaard layered series. Geochimica et Cosmochimica Acta 38, 1549-1577.

Pena dos Reis, R., Pimentel, N., Garcia, A., 2011. The Lusitanian Basin (Portugal): stratigraphic analysis and geodynamic evolution. Boletim de Geociências da Petrobras 19, 23-52.

Pena dos Reis, R., Pimentel, N., 2014. **Analysis of the petroleum systems of the Lusitanian Basin (Western Iberian Margin) – A tool for deep offshore exploration,** in: Sedimentary Basins: Origin, Depositional Histories and Petroleum Systems. 33rd Annual GCSSEPM Foundation Bob F. Perkins Research Conference, Houston, Texas.

Pereira, R., Alves, T., 2011. Margin segmentation prior to continental break-up: A seismic-stratigraphic record of multiphased rifting in the North Atlantic (Southwest Iberia). Tectonophysics 505, 17-34.

Pereira, R., Alves, T., 2012. Tectono-stratigraphic signature of multiphased rifting on divergent margins (deep-offshore Southwest Iberia, North Atlantic). Tectonics 31(4), TC4001, doi: 10.1029/2011TC003001

Pinheiro, L.M., Wilson, R.C.L., Pena dos Reis, R., Whitmarsh, R.B., Ribeiro, A., 1996. The western Iberia margin: a geophysical and geological overview, in: Whitmarsh,

R.B., Sawyer, D.S., Klaus, A., Masson, D.G. (Eds), Proceedings of the Ocean Drilling Program, Scientific Results 149, pp. 3-22.

Presnall, D.C., Dixon, S.A., Dixon, J.R., O'Donnell, T.H., Brenner, N.L., Schrock, R.L., Dycus, D.W., 1978. Liquidus phase relations on the join diopside-forsterite-anorthite from 1 atm to 20 kbar: their bearing on the generation and crystallization of basaltic magma. Contributions to Mineralogy and Petrology 66, 203-220.

Rapaille, C., Marzoli, A., Bertrand, H., Féraud, G., Reinsberg, L., Fontignie, D., 2003. Geochemistry and $^{40}Ar/^{39}Ar$ of the European part of the Central Atlantic Magmatic Province. European Union of Geosciences, Nice, p. 11791.

Rasmussen, E.S., Lomholt, S., Andersen, C., Vejbaek, O.V., 1998. Aspects of the structural evolution of the Lusitanian Basin in Portugal and the shelf and slope area offshore Portugal. Tectonophysics 300, 199-181.

Renne, P.R., Deino, A.D., Hames, W.E., Heizler, M.T., Hemming, RH., Hodges, K.V., Koppers, A.A.P., Mark, D.F., Morgan, L.E., Phillips, D., Singer, B.S., Turrin, B.D., Villa, I.M., Villeneuve, M., Wijbrans, J.R., 2009. Data reporting norms for 40Ar/39Ar geochronology. Quaternary Geochronology 4, 346-352.

Reston, T.J., 2009. The structure evolution and symmetry of the magma-poor rifted margins of North and Central Atlantic: a synthesis. Tectonophysics 468, 6-27.

Ribeiro, A., Antunes, M.T., Ferreira, M., Rocha, R.B., Soares, A., Zbyszewski, G., Almeida, F.M., Carvalho, D., Monteiro, J.H., 1979. Introduction à la géologie génerale du Portugal. Serviços Geológicos de Portugal, Lisboa, 114 pp.

Ribeiro, A., Kullberg, M.C., Kullberg, J.C., Manupella, G., Phipps, S., 1990. A review of Alpine tectonics in Portugal: foreland detachment in basement and cover rocks. Tectonophysics 184, 357-366.

Rickl, J., Frank, M., Halliday, A.N., 2009. The hafnium-neodymium isotopic composition of Atlantic seawater. Earth and Planetary Science Letters 280, 118-127.

Robinson, J.A.C., Wood, B.J., 1998. The depth of the spinel to garnet transition at the peridotite solidus. Earth and Planetary Science Letters 164, 277-284.

Rock, N.M.S., 1982. The Late Cretaceous Alkaline Igneous Province in the Iberian Peninsula, and its tectonic significance. Lithos 15, 111-131.

Rosenbaum, G., Lister, G., Duboz, C., 2002. Relative motions of Africa, Iberia and Europe during Alpine orogeny. Tectonophysics 359, 117-129.

Ryan, M.P., 1994. Neutral buoyancy controlled magma transport and storage in mid-ocean ridge magma reservoirs and their sheeted-dyke complex: a summary of basic relationships, in: Ryan, M.P. (Ed.), Magmatic Systems, Academic Press, New York, Vol. 57, 97-138.

Sack, R.O., Walker, D., Carmichael, I.S.E., 1987. Experimental petrology of alkalic lavas: constraints on cotectics of multiple saturation in natural basic liquids. Contributions to Mineralogy and Petrology 96, 1-23.

Scharer, U., Girardeau, J., Cornen, G., Boillot, G., 2000. 138-121 Ma asthenospheric magmatism prior to continental break-up in the North Atlantic and geodynamic implications. Earth and Planetary Science Letters 181, 555-572.

Seifert, K.E., Brunotte, D., 1996. Geochemistry of serpentinized mantle peridotite from site 897 in the Iberia abyssal plain, in: Whitmarsh, R.B., Sawyer, D.S., Klaus, A., Masson, D.G. (Eds), Proceedings of the Ocean Drilling Program, Scientific Results 149, pp. 413-421.

Seifert, K., Gibson, I., Weis, D., Brunotte, D., 1996. Geochemistry of metamorphosed cumulate gabbros from hole 900A, Iberia Abyssal Plain, in: Whitmarsh, R.B., Sawyer, D.S., Klaus, A., Masson, D.G. (Eds), Proceedings of ODP, Scientific Results 149, pp. 471-488.

Seton, M., Muller, R.D., Zahirovic, S., Gaina, C., Torsvik, T., Shephard, G., Talsma, A., Gurnis, M., Turner, M., Maus, S., Chandler, M., 2012. Global continental and ocean basin reconstructions since 200 Ma. Earth Science Reviews 13, 212-270.

Shaw, D. M., 2006. Trace Elements in Magmas. A Theoretical Treatment. Cambridge University Press, 243 pp.

Sibuet, J.C., Srivastava, S., Manatschal, G., 2007. Exhumed mantle-forming transitional crust in the Newfoundland-Iberia rift and associated magnetic anomalies. Journal of Geophysical Research 112, B06105, doi: 10.1029/2005JB003856.

Srivastava, S., Sibuet, J.-C., Cande, S., Roest, W.R., Reid, I.R., 2000. Magnetic evidence for slow seafloor spreading during the formation of the Newfoundland and Iberia margins. Earth and Planetary Science Letters 182, 61-76.

Stapel, G., Cloetingh, S., Pronk, B., 1996. Quantitative subsidence analysis of the Mesozoic evolution of the Lusitanian Basin (western Iberian margin). Tectonophysics 266, 493-507.

Steuber, T., Viezer, J., 2003. Phanerozoic record of plate tectonic control of seawater chemistry and carbonate sedimentation. Geology 30, 1123-1126.

Soares, D.M., Alves, T.M., Terrinha, P., 2012. The breakup sequence and associated lithospheric breakup surface: Their significance in the context of rifted continental margins (West Iberia and Newfoundland margins, North Atlantic). Earth and Planetary Science Letters, 355-6, 311-326.

Stein, M., and Hofmann. A., 1992. Fossil plume head beneath the Arabian lithosphere? Earth and Planetary Science Letters, 114, 193-209.

Sun, S.-s., McDonough, W.F., 1989. Chemical and isotopic systematics of ocean basalts; implications for mantle composition and processes. Geological Society, London, Special Publications 42, 313-345.

Taisne, B., Jaupart, C., 2011. Magma expansion and fragmentation in a propagating dyke. Earth and Planetary Science Letters 301, 146-152.

Tanaka T., Togashi S., Kamioka H.,Amakawa H.,Kagami H.,Hamamoto T., Yuhara M., Orihashi Y.,Yoneda S.,Shimizu H., Kunimaru T., Takahashi K., Yanagi T.,Nakano T., Fujimaki H., Shinjo R., Asahara Y., Tanimizu M., Dragusanu C., 2000. JNdi-1: a neodymium isotopic reference in consistency with LaJolla neodymium. Chemical Geology 168, 279-281.

Tesauro, M., Kaban, M.K., Cloetingh, S.A.P.L., 2013. A new thermal and rheological model of the European lithosphere. Tectonophysics 476, 478–495.

Teixeira, B.A., Pimentel, N., Pena dos Reis, R., 2012. Low lithospheric stretching in an Atlantic margin basin: the Lusitanian Basin (West Iberia, Portugal). Abstracts III Atlantic Conjugate Margins Conference, PIP (Ireland), pp. 190-191.

Terrinha, P., Ribeiro, C., Kullberg, J.C., Lopes, C., Rocha, A. Ribeiro, R., 2002. Compressive episodes and faunal isolation during rifting, Southwest Iberia: Journal of Geology 110, 101–113.

Terrinha, P., Pinheiro, L.M., Henriet, J.-P., Matias, L., Ivanov, M. K., Monteiro, J. H., Akhmetzhanov, A., Volkonskaya, A., Cunha, T., Shaskin, P., Rovere, M., TTR10 Shipboard Scientific Party (2003) - Tsunamigenic-seismogenic structures, neotectonics, sedimentary processes and slope instability on the southwest Portuguese Margin. Marine Geology 195, 55-73.

Thirlwall M.F., 1991. Long-term reproducibility of multicollector Sr and Nd isotope ratio analysis. Chemical Geology 94, 85-104.

Thy, P., Lofgren, G.E., 1994. Experimental constraints on the low-pressure evolution of transitional and mildly alkalic basalts: the effect of Fe-Ti oxide minerals and the origin of basaltic andesites. Contributions to Mineralogy and Petrolology 116, 340-351.

Thompson, R.N., 1984. Dispatches from the basalt front. 1. Experiments. Proceedings of the Geological Association 95, 249-262.

Tucholke, B.E., Sawyer, D.S., Sibuet, J.C., 2007. Breakup of the Newfoundland-Iberia rift. Geological Society Special Publications 282, 9–46.

Tucholke, B.E., Whitmarsh, R.B., 2012. The Newfoundland-Iberia conjugate rifted margins, in: Roberts, D.G., Bally, A.W. (Eds.), Regional geology and tectonics: Phanerozoic passive margins, cratonic basins and global tectonic maps, Elsevier, Amsterdam, Vol. 1C, 342-382, doi: 10.1016/B978-0-444-56357-6.00009-3

Ubide, T., Wijbrans, J.R., Galé, C., Arranz, E., Lago, M., Larrea, P., 2014. Age of the Cretaceous alkaline magmatism in northeastern Iberia: Implications for the Alpine cycle in the Pyrenees. Tectonics, 33, 1444-1460, doi: 10.1002/2013TC003511.

Uphoff, T. 2005. Subsalt, pre-Jurassic, exploration play in the northern Lusitanian basin of Portugal. American Association of Petroleum Geologists Bulletin 89(6), 699-714.

Verati, C., Rapaille, C., Féraud, G., Marzoli, A., Bertrand, H., Youbi, N., 2007. $^{40}Ar/^{39}Ar$ ages and duration of the Central Atlantic Magmatic Province volcanism in Marocco and Portugal and its relation to the Triassic-Jurassic boundary. Palaeogeography, Palaeoclimatology, Palaeoecology 244, 308-325.

Wang, K., Plank, T., Walker, J.D., Smith, E.I., 2002. A mantle melting profile across the Basin and Range, SW USA. Journal of Geophysical Research 107, B1, 2017, doi: 10.1029/2001JB000209

Watson, S., McKenzie, D., 1991. Melt generation by plumes: a study of Hawaiian volcanism. Journal of Petrology 32, 501-537.

Whitmarsh, R.B., Manatschal, G., Minshull, T.A., 2001. Evolution of magma-poor continental margins from rifting to seafloor spreading. Nature 413, 150-154.

Wilson, R.C.L., Hiscott, R.N., Willis, M.G., Gradstein, F.M., 1989. The Lusitanian Basin of West-Central Portugal: Mesozoic and Tertiary tectonic, stratigraphic and subsidence history. In: Tanard, A.J., Balkwill, H.R. (eds), Extensional tectonics and stratigraphy of the North Atlantic margins, American Association of Petroleum Geologists Memoir 46, 341-361.

Wilson, R.L.C., Sawyer, D.S., Whitmarsh, R.B., Zerong, J., Carbonell, J., 1996. Seismic stratigraphy and tectonic history of the Iberia Abyssal Plain, in: Whitmarsh, R.B., Sawyer, D.S., Klaus, A., Masson, D.G. (Eds.), Proceedings of the Ocean Drilling Programme, Scientific Results 149, 617–633, doi: 10.2973/odp.proc.sr.149.245.1996

Yoder, H.S., Tilley, C.E., 1962. Origin of basalt magmas: an experimental study of natural and synthetic rock systems. Journal of Petrology 3, 342-532.

Figure captions

Fig. 1 - Geological sketch of the Lusitanian Basin presenting the sampling location of the rocks used in this study (simplified and adapted from Carta Geológica de Portugal at a 1/1,000,000 scale, LNEG, 2010). The insert shows the location of the main map (square) in Portugal, while the Mesozoic Lusitanian (LB) and Algarve (AB) basins are shown as grey areas. The location and extension of the Mesozoic peridotite ridge (thick black line off the Galicia bank) was taken from Beslier et al. (1996) and Chazot et al. (2005). The major faults referenced in the text are also shown: AF – Aveiro Fault, PTF – Porto-Tomar Fault; NF – Nazaré Fault; TVF – Torres Vedras Fault; TagVF - Tagus Valley Fault; ArriF – Arrife Fault; SPNF – Setúbal-Pinhal Novo Fault; ArrF – Arrábida Fault; MF – Messejana Fault. Black circles (northern rocks) and white circles (southern rocks) locate the samples used in this study; white rectangles with the PT reference represent the location of the samples studied by Grange et al. (2008).

Fig. 2 - Simplified lithostratigraphic chart of the Lusitanian Basin indicating the main formations or groups, according to their predominant lithology and age. Magmatic occurrences are also represented by age and location. Note that the horizontal axis represents geographical space (south to north), whereas the vertical axis represents stratigraphic time (stages and absolute ages; Cohen et al., 2013; updated). Figure adapted from Pena dos Reis and Pimentel, 2014 (see also references therein).

Fig. 3 - Step-heating $^{40}Ar/^{39}Ar$ apparent age spectra for the dated samples. Reported errors for plateau ages are 2σ. Steps used for the plateau age calculation are presented as filled and also indicated by a left-right arrow. See also Table 1. Inverse isochron diagrams are shown as Supplementary Material - S2.

Fig. 4 - Total alkali–silica (TAS) diagram (LeBas et al., 1986) from the second magmatic cycle onshore WIM. The boundary line between the alkaline and sub-alkaline fields is from Irvine and Baragar (1971). For comparison purposes, selected samples (MgO > 6 wt %) of the first (CAMP: Callegaro et al. 2014; Martins et al. 2008; Cebriá et al., 2003) and third (Martins, 1999; Miranda, 2010; Grange et al. 2010) magmatic cycles are also plotted.

Fig. 5 – Selected rare earth elements **(A)** and trace-element **(B)** patterns normalized, respectively, to chondrite and primordial mantle compositions (McDonough and Sun, 1995). For comparison, in Fig. 5B, an N-MORB (Sun and McDonough, 1989) pattern is also shown.

Fig. 6 - Nd initial isotopic ratios plotted against Sr initial isotopic ratios (values recalculated for 145 Ma ago). For comparative purposes, the isotopic ratios for CHUR and UR (DePaolo, 1988 and reference therein), recalculated for 145 Ma ago, and the ranges of the initial isotopic ratios from the first (CAMP: Cebriá et al., 2003) and third (Miranda, 2010) magmatic cycle of onshore WIM are also represented.

Fig. 7 - **A-** Normative compositions of the studied rocks with $(^{87}Sr/^{86}Sr)_i < 0.7052$. Ne: nepheline; Di: diopside; Ol: olivine; Hy: hypersthene; Q: quartz. The studied rocks form a suite ranging from Ne-normative to SiO_2-oversaturated rocks (See Thompson, 1984); **B**- Variation of normative compositions as a function of Ni concentration, here used as a proxy for the degree of magmatic evolution. Note that the samples characterized by

$(^{87}Sr/^{86}Sr)_i$ > 0.7052 plot clearly outside the trend defined by the unaltered rocks. **C**- Normative composition of the samples in terms of normative nepheline (Ne), olivine (Ol) and Di (diopside), as defined by Sack et al. (1987). Also plotted are the 8 to 30 kbar and 1 bar cotectic lines at QFM oxygen fugacity conditions (see Sack et al., 1987 and references therein).

Fig. 8- La vs. Th bivariate diagram. The studied samples define a linear trend characterized by an approximately constant value of Th/La, which indicates that they form a suite generated by the fractional crystallization of magmas generated from a relatively homogeneous source. However, note that the Th and La concentrations do not correlate negatively with an evolution index like Mg#. Sample BL23 was not considered for the determination of the correlation line. Only samples with $(^{87}Sr/^{86}Sr)_i$ < 0.7052 were plotted.

Fig. 9 - Ni vs. Zr diagram. The sub-horizontal trend line represents the composition of liquids resulting from the modal partial batch melting of a mantle peridotite (Ni = 3000 ppm; Zr = 15 ppm), leaving as a residue a paragenesis composed of 0.55 Ol, 0.25 Opx, 0.15 Cpx and 0.05 Gr. Degree of partial melting (F) ranges from 0.01 to 0.15. The sub-vertical trend line represents the compositional variation of an initially primary magma (Ni = 300 ppm and Zr = 50 ppm; filed star) as a consequence of the fractional crystallization of a paragenesis composed of 0.6 Ol, 0.3 Cpx, and 0.1 Plag. F represents the fraction of the remaining liquid. The distribution coefficients compiled by Shaw (2006) were used when modelling partial melting and fractional crystallization trends. Only samples with $(^{87}Sr/^{86}Sr)_i$ < 0.7052 were plotted.

Fig. 10 – (Tb/Yb)n vs. (La/Yb)n diagram showing the fields for magmas generated from garnet-lherzolite and spinel-lherzolite sources (Wang et al., 2002). Only samples with $(^{87}Sr/^{86}Sr)_i$ < 0.7052 were plotted. For comparison, the fields defined by rocks (mostly primitive) from the first (Martins et al., 2008) and third (Miranda et al., 2009; Miranda, 2010; Grange et al., 2010) magmatic cycles are also represented.

Fig. 11 - Th/Yb vs. Th/Ta diagram. The occurrence of samples with distinct values of the Ta/Yb ratio is interpreted as evidence for several distinct episodes of partial melting. Only samples with $(^{87}Sr/^{86}Sr)_i$ < 0.7052 were plotted. PM stands for the modal partial batch melting of a mantle peridotite, leaving as residue a paragenesis composed of 0.55 Ol, 0.25 Opx, 0.15 Cpx and 0.05 Gr. FC stands for the fractional crystallization of a paragenesis composed of 0.55 Ol, 0.3 Cpx, 0.14 Plag, and 0.01 (FC1) and 0.55 Ol, 0.3 Cpx, 0.10 Plag, and 0.05 Ilm (FC2). The distribution coefficients compiled by Shaw (2006) were used when modelling partial melting. Fractional crystallization trends were obtained using the partition coefficients of Adam and Green (2006), Green and Pearson (1987), McKenzie and O'Nions (1991) and Paster et al. (1987).

Fig. 12 - Ba vs. Cs bivariate diagram. Note that the dispersion observed when plotting incompatible large ion lithophile elements is at odds with the behaviour observed for high field strength elements (cf. Fig. 8).

Fig. 13 – Putative mixing line between lithosphere-derived (1st cycle) and plume-derived (3rd cycle) compositions, which could suggest a model of plume-lithosphere interaction to explain the isotopic signatures of the second cycle magmatic rocks. This hypothesis was denied based on several types of geological arguments (see main text).

Only samples with $(^{87}Sr/^{86}Sr)_i < 0.7052$ were plotted. Sample 27 from Cebriá et al. (2003) and sample RM16 from Miranda (2010) were selected as representatives of the 1st and 3rd cycles, respectively. Thick marks represent mixing increments of 10%.

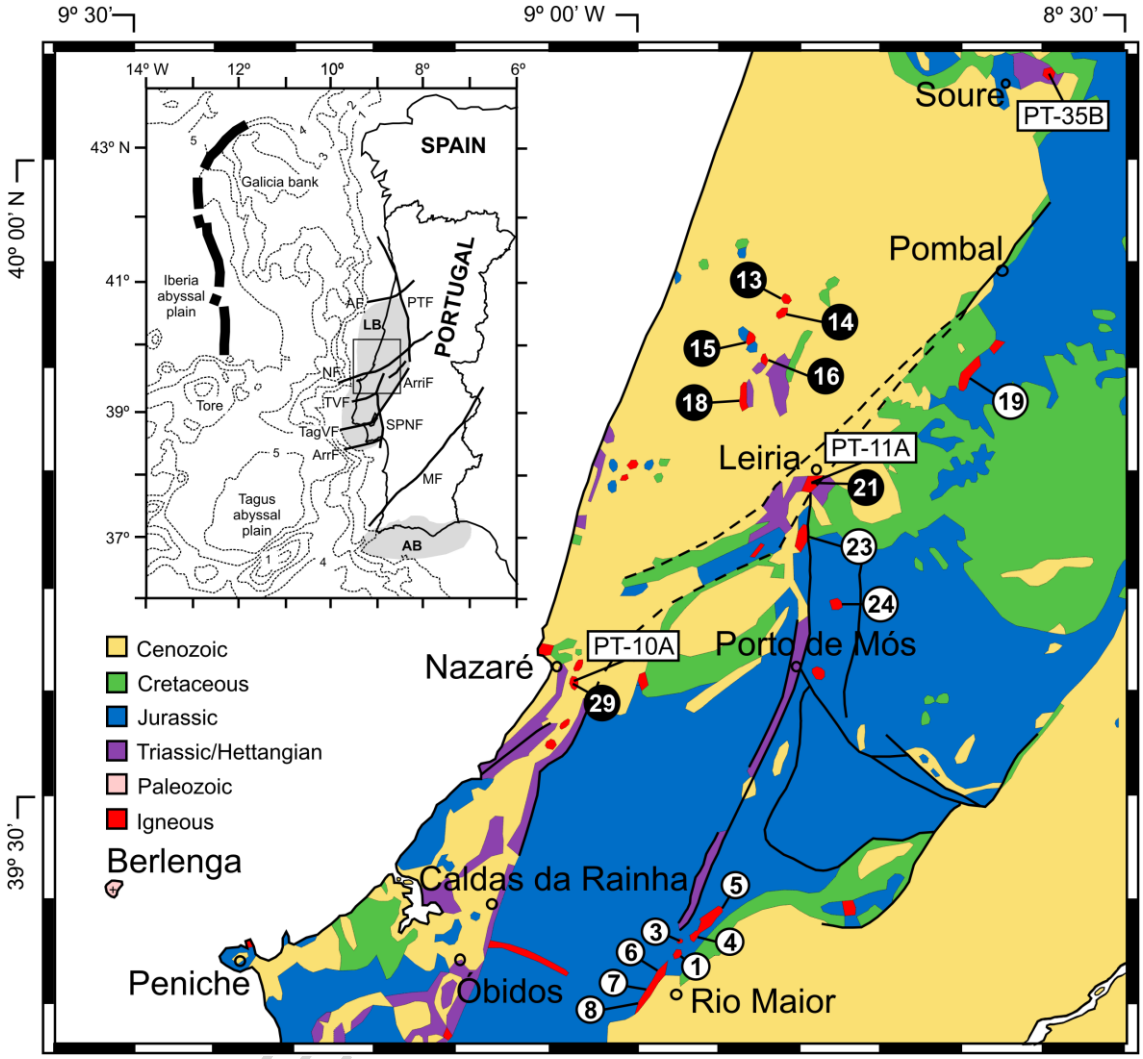

Figure 1

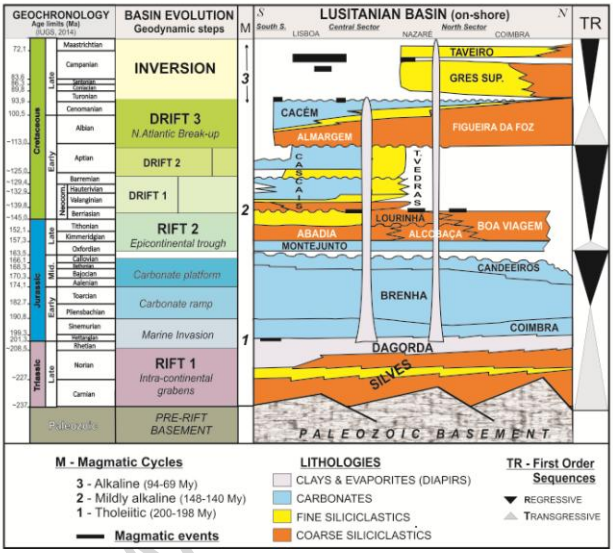

Figure 2

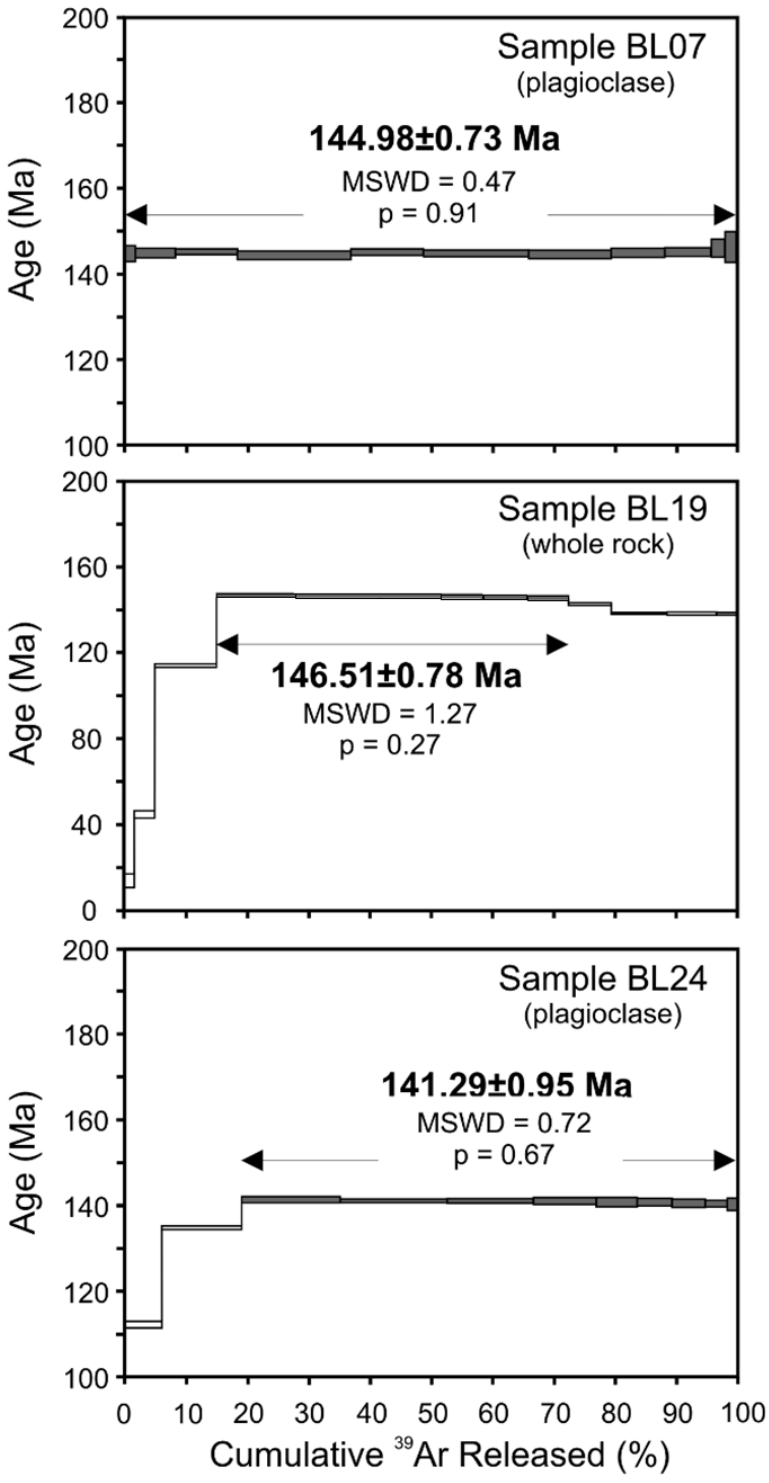

Figure 3

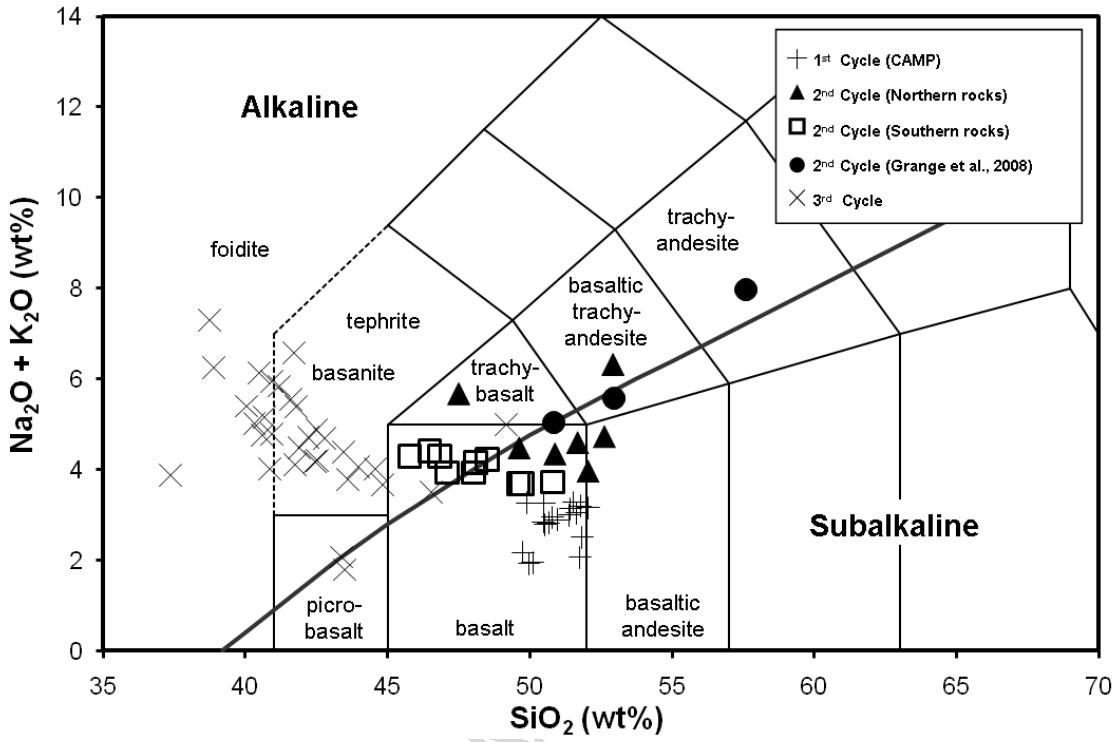

Figure 4

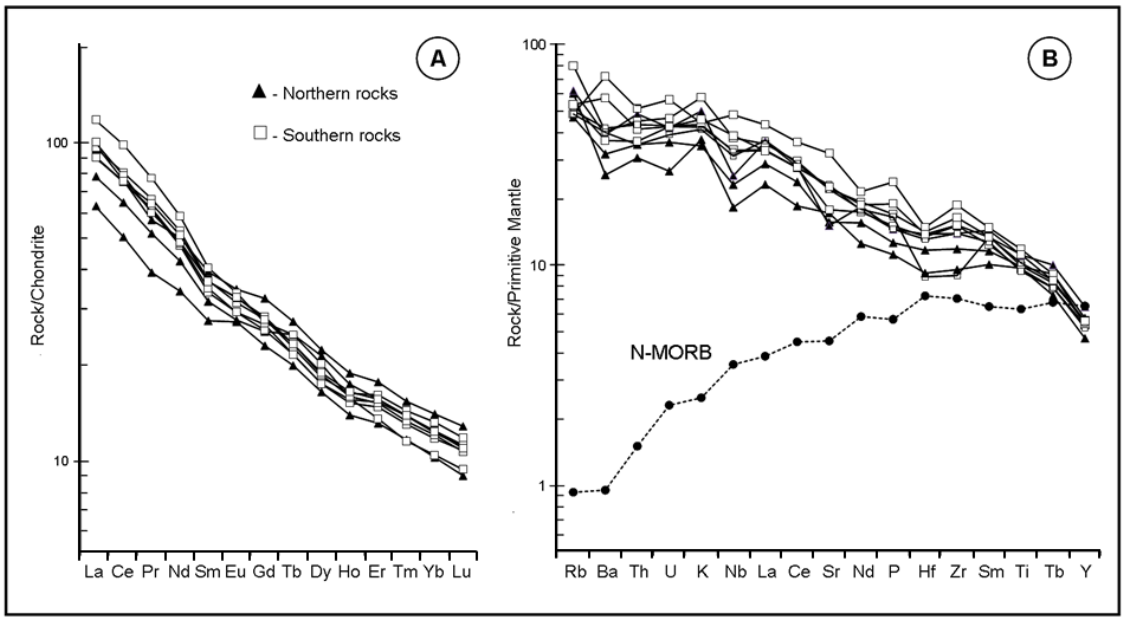

Figure 5

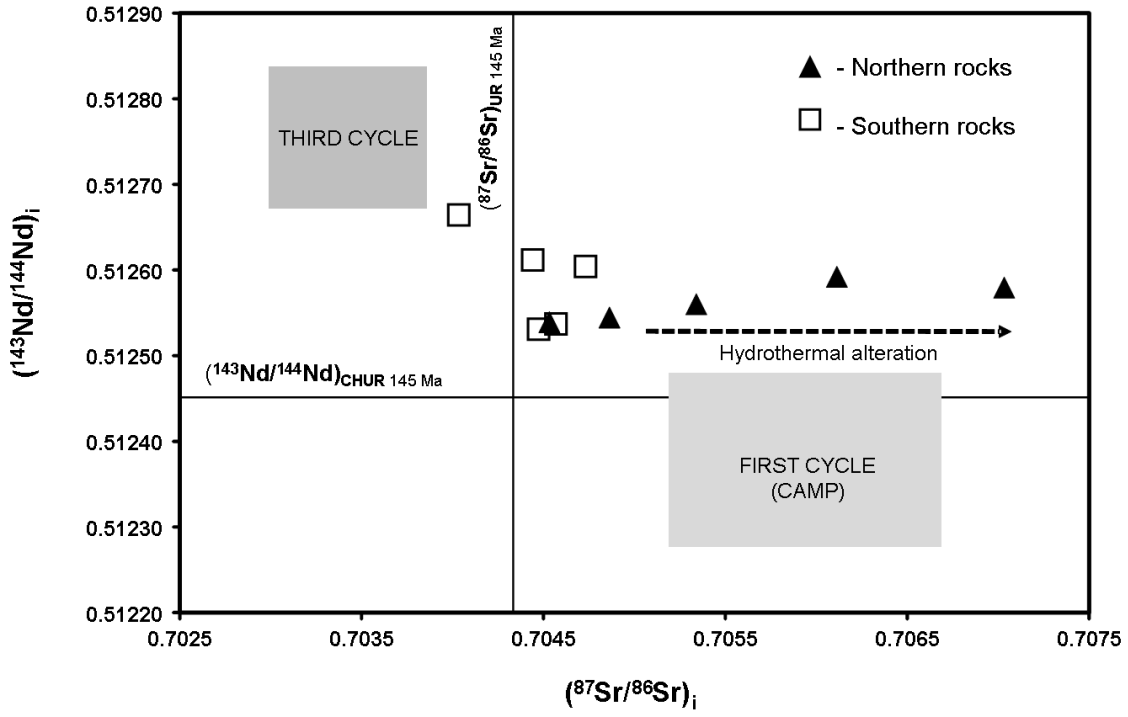

Figure 6

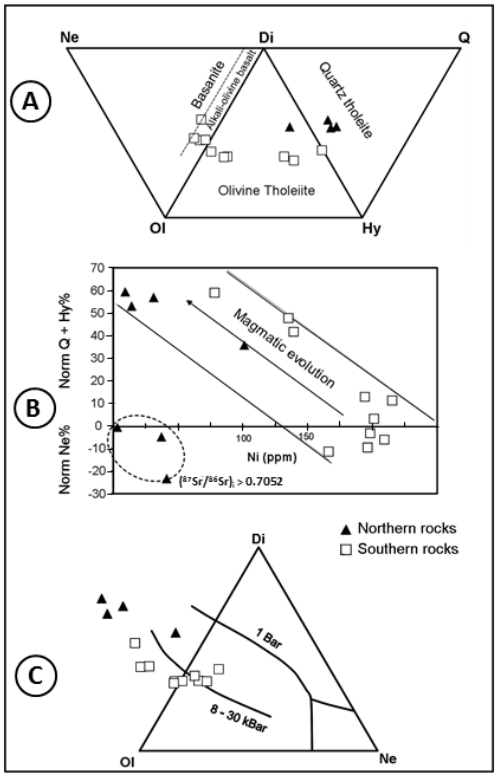

Figure 7

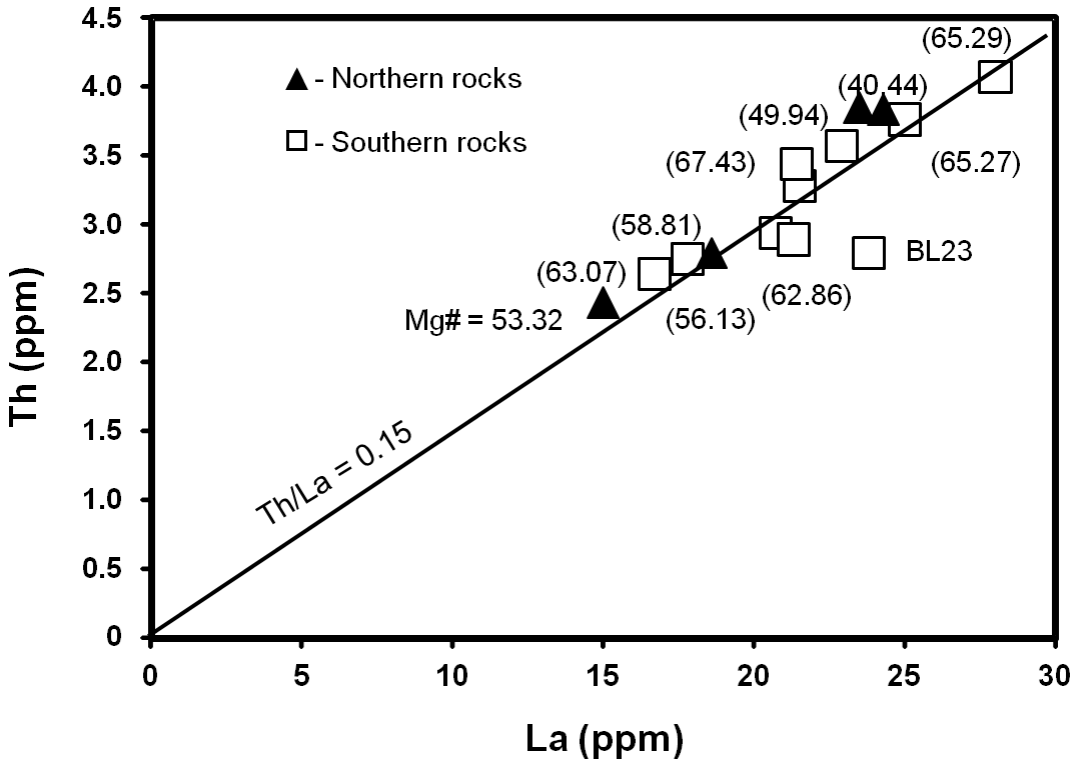

Figure 8

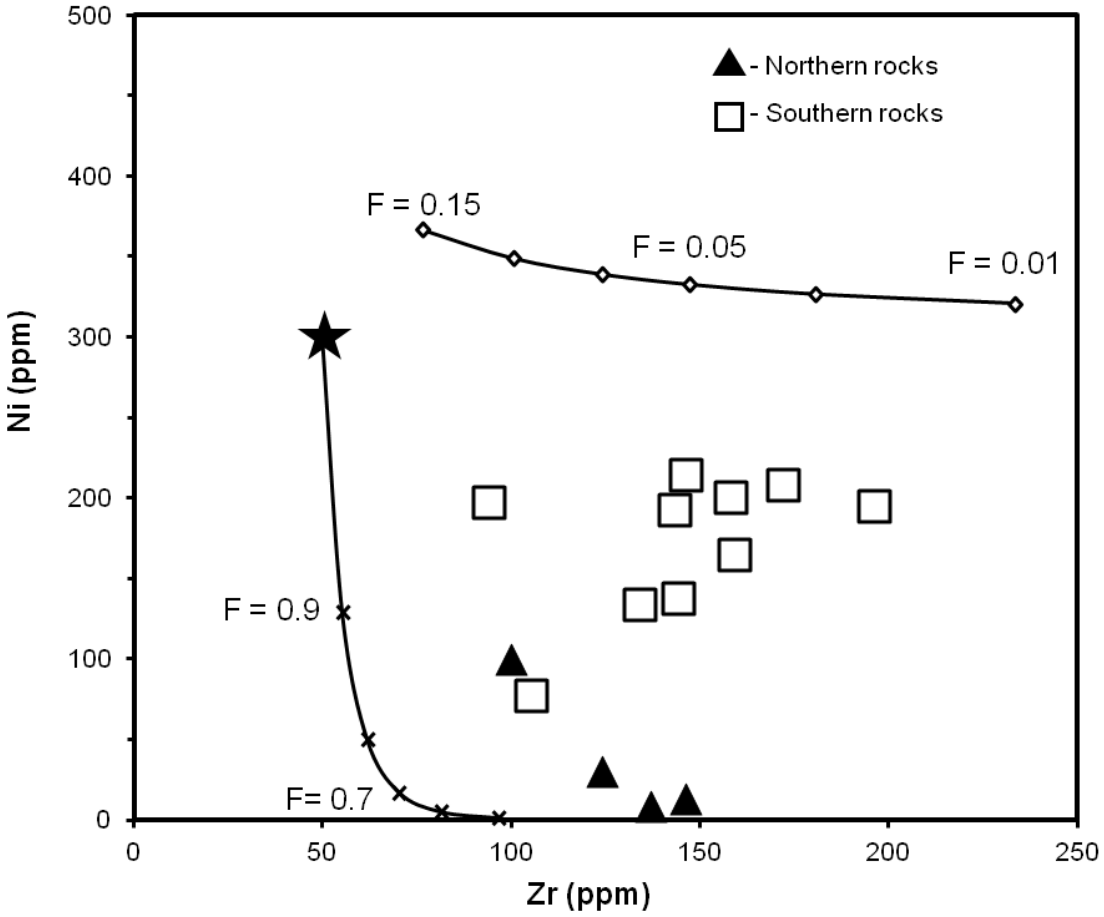

Figure 9

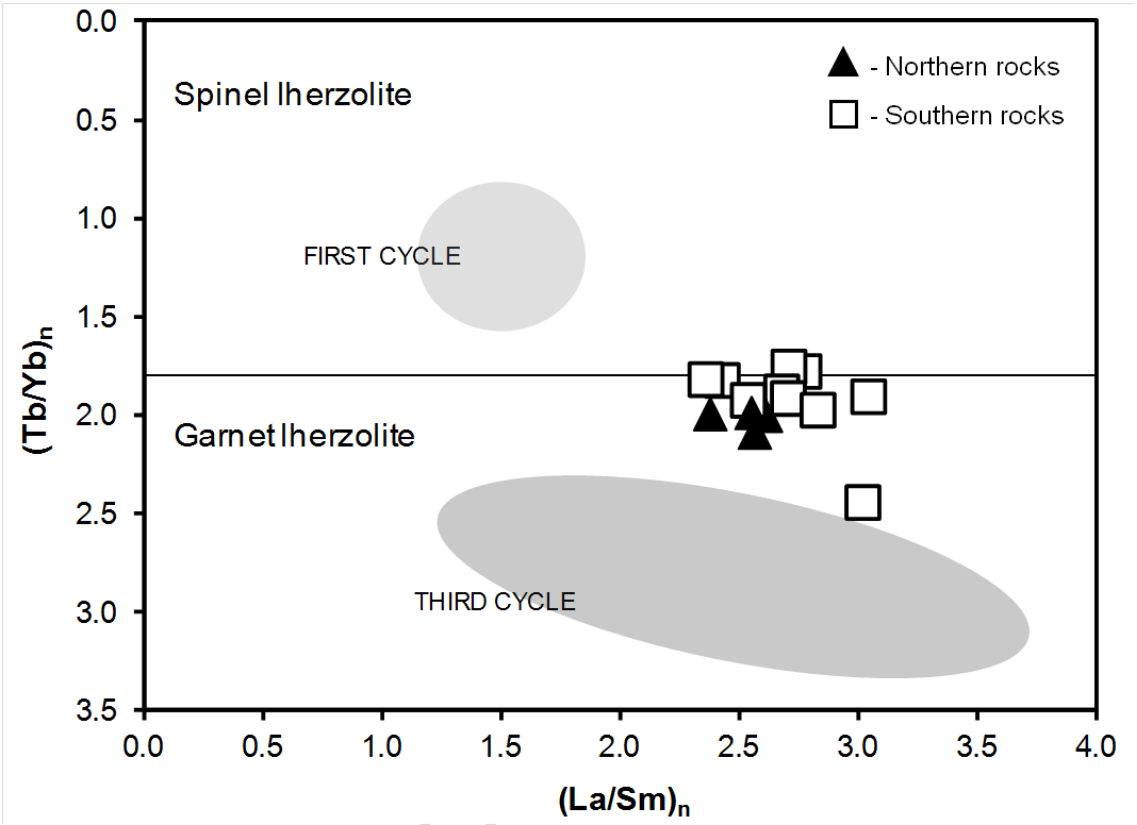

Figure 10

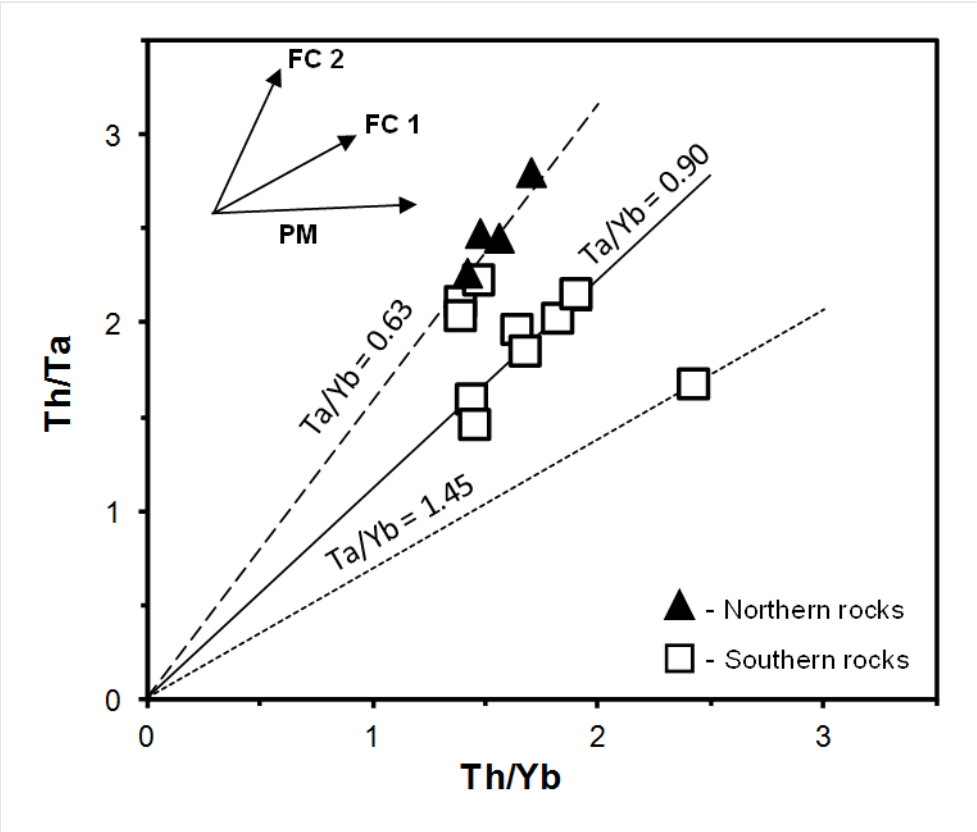

Figure 11

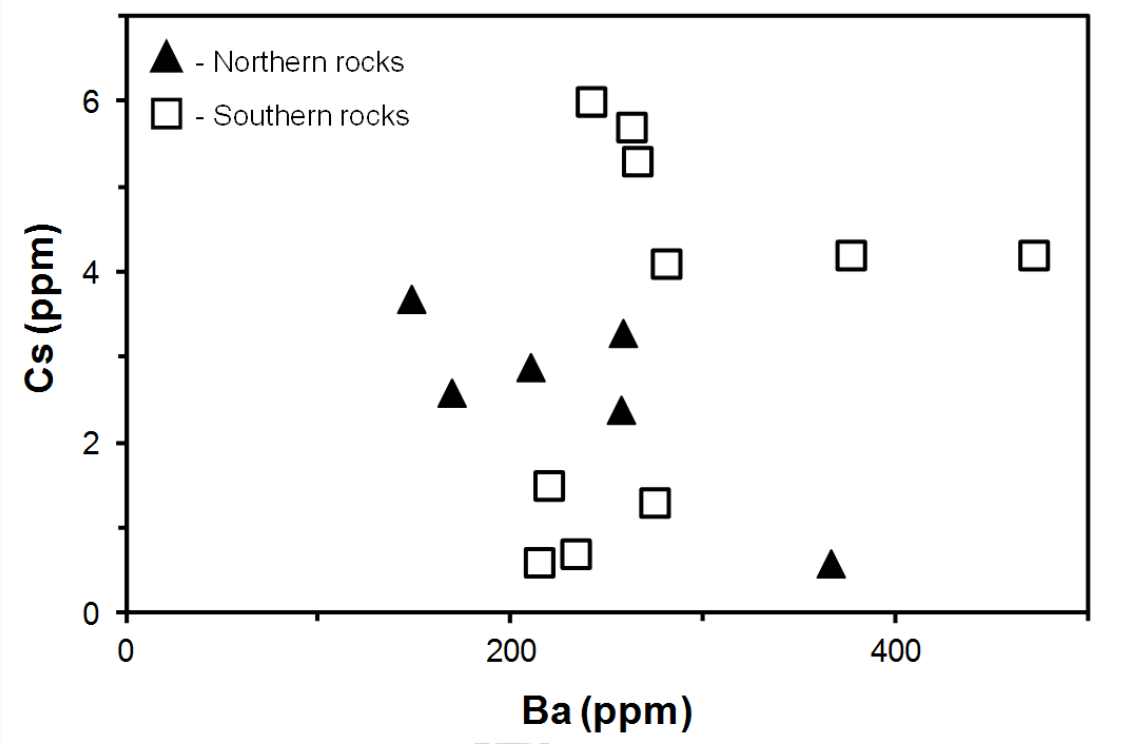

Figure 12

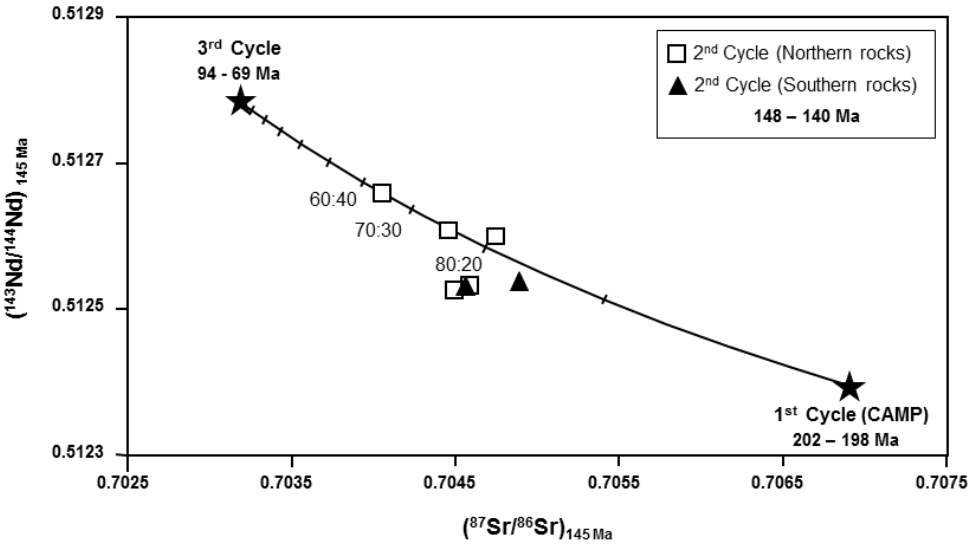

Figure 13

Table 1- Age results

Sample		**BL07** Plagioclase	**BL19** Whole rock	**BL24** Plagioclase
Plateau Characteristics	Age (Ma±2σ)	144.98±0.73	146.51±0.78	141.29±0.95
	No. Increments	11/11	6/13	9/11
	^{39}Ar (% of total)	100	57.43	81.04
	K/Ca (±2σ)	0.040±0.002	0.384±0.024	0.135±0.017
	MSDW	0.47	1.27	0.72
	p	0.91	0.27	0.67
Isocron Characteristics	Age (Ma±2σ)	144.82±0.76	146.19±0.91	141.97±1.19
	Intersection ^{40}Ar/^{39}Ar	299.05±13.36	305.75±15.75	234.01±63.30
	MSDW	0.55	1.12	0.34
	p	0.84	0.36	0.94
Sample Characteristics	Occurence	Sill	Dyke	Sill/Lacolith
	Texture	Subophitic	Porphiritic	Porphiritic
	Grain size	Average~0.5mm	Matrix<0.05mm	Matrix<0.2mm
	TAS	Basalt	Basalt	Basalt
	LOI wt%	1.38	2.08	0.92

MSDW - mean square weighted deviate
p - probability of occurrence for 95% confidence level

Table 2- Major and trace element concentrations

	Southern Rocks										Northern Rocks						
Sample	**BL01**	**BL03**	**BL04**	**BL05**	**BL06**	**BL07**	**BL08**	**BL19**	**BL23**	**BL24**	**BL13**	**BL14**	**BL15**	**BL16**	**BL18**	**BL21**	**BL29**
SiO_2 (wt.%)	47.47	46.94	45.69	46.51	47.95	49.38	49.94	43.99	46.21	45.92	50.20	50.26	50.46	52.10	45.37	47.57	51.80
TiO_2	1.93	1.93	1.99	1.88	1.89	1.94	1.90	2.37	2.05	2.24	3.10	1.95	1.98	2.23	2.31	2.15	2.13
Al_2O_3	14.12	14.27	14.02	14.07	14.29	14.62	14.99	13.90	14.03	14.71	13.85	16.51	15.36	15.49	15.84	16.28	15.35
Fe_2O_3(t)	11.98	11.73	11.85	11.54	11.49	11.95	11.33	12.35	12.15	12.17	13.43	10.50	10.50	11.07	11.40	9.58	11.44
MnO	0.18	0.19	0.21	0.18	0.19	0.19	0.18	0.18	0.17	0.19	0.17	0.13	0.19	0.16	0.06	0.13	0.08
MgO	9.63	9.76	10.34	10.22	8.39	8.73	6.92	9.94	10.06	8.81	3.90	5.13	5.34	4.39	5.36	5.12	2.18
CaO	8.13	8.44	8.94	8.35	8.40	8.80	9.14	8.77	9.27	10.02	7.74	9.80	9.05	8.61	9.40	10.50	8.07
Na_2O	2.82	2.84	2.52	2.56	2.49	2.66	2.70	2.85	2.67	3.03	2.70	3.23	2.85	3.25	4.68	3.59	5.66
K_2O	1.31	1.22	1.66	1.25	1.06	1.02	0.96	1.27	1.19	1.32	1.77	1.07	1.00	1.44	0.75	0.71	0.54
P_2O_5	0.34	0.31	0.35	0.30	0.27	0.28	0.27	0.49	0.34	0.39	0.31	0.23	0.26	0.30	0.38	0.26	0.66
LOI	1.71	1.10	1.25	1.75	2.00	1.38	1.10	1.78	0.80	0.92	1.25	1.52	1.74	1.59	3.40	2.47	1.11
Total	99.60	98.74	98.84	98.60	98.42	100.9	99.42	97.88	98.94	99.70	98.41	100.3	98.72	100.6	98.96	98.35	99.02
#Mg	65.27	66.04	67.10	67.43	63.06	63.07	58.81	65.29	65.93	62.86	40.43	53.32	56.13	49.94	54.19	55.54	33.17
Sc (ppm)	23	25	25	23	24	24	23	21	25	26	24	23	23	23	25	25	13
V	229	239	241	223	225	224	224	246	254	256	321	234	213	232	263	241	129
Cr	290	370	410	390	330	350	230	290	310	300	BDL	130	240	70	120	310	BDL
Co	44	53	54	53	45	49	34	50	43	48	28	27	31	25	26	30	22
Ni	193	200	208	214	134	138	77	195	197	165	8	100	30	13	40	36	2
Cu	47	48	51	44	39	34	26	34	41	44	12	12	3	13	5	4	14
Zn	81	81	114	80	83	80	82	88	76	78	84	59	39	70	21	38	41
S	430	430	420	340	100	260	360	180	410	530	110	1440	1100	1170	2560	220	50
Rb	36	32	48	30	27	26	24	29	29	32	60	36	28	37	30	21	10
Sr	406	354	440	459	296	318	344	638	438	450	300	342	311	300	411	527	421
Y	23.3	23	24.1	22.3	22	23.4	23.9	23.3	23.4	24	30.9	20	24.7	27.8	25	20.6	41.4
Zr	143	158	172	146	134	144	105	196	94	159	137	100	124	146	162	122	293
Nb	21.8	21.8	24.8	21.5	16.3	17.2	15.7	31.5	20.5	25.4	18.8	12	15.2	16.7	23.6	14.4	40.6
Cs	4.1	4.2	5.3	1.3	1.5	0.6	0.7	4.2	5.7	6.0	3.3	2.6	2.9	2.4	-	3.7	0.6
Ba	281	377	266	275	220	215	234	472	263	242	258	169	210	257	226	148	366
La	25.0	21.5	22.9	21.4	16.7	17.8	20.7	28.0	23.8	21.3	24.3	15.0	18.6	23.5	28.3	14.3	29.2
Ce	50.1	46.2	49.4	46.1	36.9	39.0	42.0	60.5	48.3	46.5	49.0	31.0	39.8	46.7	55.0	32.6	68.7
Pr	5.55	5.68	6.18	5.77	4.71	5.00	4.75	7.19	5.58	5.97	5.60	3.63	4.81	5.31	6.18	4.25	9.15
Nd	22.8	21.7	24.1	22.1	18.7	20.1	19.7	26.9	22.3	23.4	23.9	15.6	19.4	23.0	24.8	17.6	36.5
Sm	5.30	5.01	5.46	5.16	4.44	4.87	4.94	5.99	5.43	5.42	6.16	4.08	4.69	5.82	5.87	4.44	8.95
Eu	1.76	1.65	1.77	1.65	1.58	1.63	1.67	1.90	1.83	1.84	2.00	1.54	1.56	1.95	1.94	1.65	2.85
Gd	5.51	5.33	5.55	5.12	4.94	5.14	5.36	5.41	5.64	5.54	6.92	4.58	5.08	6.45	5.98	4.89	9.34
Tb	0.83	0.78	0.82	0.78	0.76	0.79	0.84	0.90	0.84	0.84	1.07	0.72	0.90	0.99	0.89	0.72	1.41
Dy	4.6	4.3	4.5	4.29	4.19	4.36	4.63	4.96	4.58	4.65	5.98	4.05	5.26	5.49	4.83	4.01	7.78
Ho	0.88	0.85	0.89	0.83	0.81	0.87	0.90	0.86	0.87	0.90	1.15	0.76	0.95	1.03	0.91	0.77	1.54
Er	2.49	2.45	2.58	2.36	2.30	2.50	2.53	2.17	2.43	2.50	3.14	2.10	2.50	2.83	2.51	2.13	4.43
Tm	0.35	0.34	0.36	0.32	0.32	0.34	0.35	0.29	0.33	0.34	0.42	0.29	0.34	0.38	0.33	0.28	0.61
Yb	1.98	2.00	2.13	1.89	1.90	1.98	2.00	1.68	1.94	1.99	2.46	1.65	1.97	2.26	1.96	1.65	3.53
Lu	0.28	0.28	0.29	0.27	0.26	0.27	0.29	0.23	0.26	0.27	0.34	0.22	0.27	0.32	0.27	0.23	0.49
Hf	3.6	3.8	4.0	3.7	3.3	3.6	2.9	4.2	2.5	3.9	3.7	2.6	3.3	3.9	4.0	3.2	7.0
Ta	1.75	1.67	1.93	1.70	1.25	1.35	1.32	2.43	1.75	1.98	1.56	0.98	1.23	1.37	2.01	1.14	3.32
Tl	0.35	0.44	0.49	0.13	0.23	0.27	0.06	0.06	0.11	0.19	0.13	0.33	0.10	0.10	0.22	0.36	0.12
Th	3.76	3.28	3.57	3.44	2.64	2.75	2.94	4.07	2.79	2.89	3.83	2.43	2.79	3.84	3.56	2.22	6.29
U	0.95	0.86	0.94	0.87	0.69	0.73	0.77	1.14	0.79	0.86	0.82	0.54	0.73	0.85	1.19	0.49	1.24

- Not analysed

Table 3- Sr and Nd isotope ratios of selected samples. Northern samples: shaded; Southern samples: unshaded.

Sample	Sr (ppm)	Rb(ppm)	$^{87}Rb/^{86}Sr$	Error(2σ)	$^{87}Sr/^{86}Sr$	Error(2σ)	$(^{87}Sr/^{86}Sr)_i$	
BL04	440	48	0.316	0.009	0.705091	0.000025	0.704441	
BL07	318	26	0.236	0.007	0.704961	0.000028	0.704474	
BL08	344	24	0.202	0.006	0.704985	0.000030	0.704569	
BL19	638	29	0.131	0.004	0.705003	0.000027	0.704732	
BL24	450	32	0.206	0.006	0.704458	0.000024	0.704034	
BL13	300	60	0.579	0.016	0.706056	0.000031	0.704863	
BL16	300	37	0.357	0.010	0.705268	0.000031	0.704533	
BL18	411	30	0.2112	0.006	0.707469	0.000028	0.707034	
BL21	527	21	0.115	0.003	0706351	0.000040	0.706114	
BL29	421	10	0.0687	0.0019	0.705481	0.000030	0.705340	

Sample	Nd(ppm)	Sm(ppm)	$^{147}Sm/^{144}Nd$	Error(2σ)	$^{143}Nd/^{144}Nd$	Error(2σ)	$(^{143}Nd/^{144}Nd)_i$	ε_i
BL04	24.0	5.46	0.138	0.004	0.512743	0.000014	0.512612	3.1
BL07	20.0	4.87	0.147	0.004	0.512671	0.000017	0.512531	1.6
BL08	19.0	4.94	0.157	0.004	0.512686	0.000009	0.512537	1.7
BL19	27.0	5.99	0.134	0.004	0.512731	0.000018	0.512604	3.0
BL24	23.0	5.42	0.143	0.004	0.512800	0.000009	0.512664	4.2
BL13	23.9	6.16	0.156	0.004	0.512693	0.000013	0.512545	1.8
BL16	23.0	5.82	0.153	0.004	0.512685	0.000012	0.512539	1.7
BL18	24.0	5.87	0.148	0.004	0.512720	0.000013	0.512580	2.5
BL21	17.6	4.44	0.153	0.004	0.512737	0.000017	0.512592	2.7
BL29	36.5	8.95	0.148	0.004	0.512701	0.000015	0.512560	2.1

Table 4- Published ages for second cycle rocks

Outcrop	Location	Method	Sample	Age (Ma)	Authors
Serra de Todo o Mundo	Southern	K-Ar		134±3	Ferreira & Macedo (1983)
		Ar-Ar	Plagiclase	144.98±0.73	**This work**
Alcobertas	Southern	K-Ar		133±3	Ferreira & Macedo (1983)
Alqueidão da Serra	Southern	K-Ar		140±3	Ferreira & Macedo (1983)
		Ar-Ar	Plagioclase	141.29±0.95	**This work**
Vermoil	Southern	K-Ar		144±2	Ferreira & Macedo (1983)
		Ar-Ar	WR	146.51±0.78	**This work**
Codiceira	Northern	K-Ar		165±3	Ferreira & Macedo (1983)
Soure	Northern	K-Ar		159±3	Ferreira & Macedo (1983)
		U-Pb	Titanite	145.3±1.4	Grange *et al.* (2008)
Leiria	Northern	U-Pb	Titanite	142.3±1.0	Grange *et al.* (2008)
S. Bartolomeu	Northern	U-Pb	Titanite	146.5±1.6	Grange *et al.* (2008)

In the discussion only data obtained by Ar-Ar and U-Pb methods were considered valid.

Table 5- Compositions of Hettangian sediments adjacent to Monte Real sill (BL18)

	Na_2O (wt.%)	**Rb** (ppm)	**Sr** (ppm)	**Sm** (ppm)	**Nd** (ppm)	**$(^{87}Sr/^{86}Sr)_{145}$**	**$(^{143}Nd/^{144}Nd)_{145}$**
Clay	0.15	205	106	6.21	29.9	0.720302	0.512059
Dolomite	0.18	48	99	8.27	18.7	0.707242	0.512032
Limestone	0.02	7	184	1.18	5.82	0.707847	0.511992
Gypsum	<0.01	<1	151	0.03	0.14	0.708635*	-
Rock Salt	48.47	<1	17	0.04	0.13	0.708606*	-

*- $(^{87}Sr/^{86}Sr)_{145}$ is assumed to be similar to present day values, given the “absence” of Rb.

Highlights

- In the West Iberian Margin, onshore magmatism occurred between 148 and 140 Ma.
- This is distinct from cycles that occurred at the Lower Jurassic and Upper Cretaceous times.
- Magmas were generated from garnet lherzolite and evolved at a relatively high pressure.
- Some rocks evidence post-magmatic processes involving Jurassic evaporite materials.